ACS APPLIED BIO MATERIALS

www.acsabm.org Article

Pair of Functional Polyesters That Are Photo-Cross-Linkable and Electrospinnable to Engineer Elastomeric Scaffolds with Tunable Structure and Properties

Xiaochu Ding,* Zhongtian Zhang, Christopher Kluka, Saad Asim, James Manuel, Bruce P. Lee, Jingfeng Jiang, Patricia A. Heiden, Caryn L. Heldt, and Muhammad Rizwan

Cite This: *ACS Appl. Bio Mater.* 2024, 7, 863−878 Read Online

ACCESS | Metrics & More | Article Recommendations | Supporting Information

ABSTRACT: A pair of alkyne- and thiol-functionalized polyesters are designed to engineer elastomeric scaffolds with a wide range of tunable material properties (e.g., thermal, degradation, and mechanical properties) for different tissues, given their different host responses, mechanics, and regenerative capacities. The two prepolymers are quickly photo-cross-linkable through thiol-yne click chemistry to form robust elastomers with small permanent deformations. The elastic moduli can be easily tuned between 0.96 ± 0.18 and 7.5 ± 2.0 MPa, and in vitro degradation is mediated from hours up to days by adjusting the prepolymer weight ratios. These elastomers bear free hydroxyl and thiol groups with a water contact angle of less than 85.6 ± 3.58 degrees, indicating a hydrophilic nature. The elastomer is compatible with NIH/3T3 fibroblast cells with cell viability reaching 88 ± 8.7% relative to the TCPS control at 48 h incubation. Differing from prior soft elastomers, a mixture of the two prepolymers without a carrying polymer is electrospinnable and UV-cross-linkable to fabricate elastic fibrous scaffolds for soft tissues. The designed prepolymer pair can thus ease the fabrication of elastic fibrous conduits, leading to potential use as a resorbable synthetic graft. The elastomers could find use in other tissue engineering applications as well.

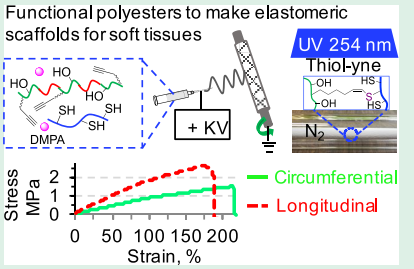

KEYWORDS: *biodegradable and bioresorbable polyesters, elastomers, thiol-yne click chemistry, synthetic vascular grafts, electrospinning*

1. INTRODUCTION

Biocompatible and biodegradable polyester elastomers have shown wide applications in tissue engineering, such as nerve conduits, cardiac patches, and synthetic vascular grafts.[1−5] For tissue engineering applications, different tissues and animals typically show different host responses, mechanical properties, and regenerative capacities.[6−8] Therefore, the elastomers with appropriate hydrophilicity, robust elasticity, and tunable material properties (e.g., degradation, mechanical properties) are preferred to engineer scaffolds for different applications. An elastomer with a water contact angle of less than 85 degrees is typically considered to be hydrophilic which will allow cell infiltration, adhesion, and proliferation in the scaffolds for remodeling.[5,9,10] In addition, an elastomer with robust elasticity is desired to undergo reversible deformations, dissipate stress exerted on the scaffolds, and help retain the scaffold integrity to guide tissue growth in a mechanically dynamic environment.[11,12] Further, a scaffold with an appropriate degradation rate is preferred to avoid immature tissue regeneration or complications such as foreign body reactions caused by either too quick or too slow degradation of the scaffold.[5,13,14] Finally, mechanical match with native tissues is important to provide sufficient mechanical support for tissue regeneration and at the same time avoid mechanical irritation by mismatch.[15−17] When it comes to engineering bioresorbable synthetic grafts for in situ arterial regeneration, we hypothesize that the designed grafts need to simultaneously possess features of appropriate hydrophilicity and degradation rate, robust elasticity, and suitable mechanical properties together with good biocompatibility and bioresorbability. These features likely play synergistic roles in graft regeneration.[5,14,18−22] In addition, an electrospinnable and quickly cross-linkable soft polyester elastomer will make the material feasible to fabricate elastic fibrous conduits as resorbable grafts for preclinical studies in different animal models.[23] To our knowledge, no elastomer has been designed to simultaneously satisfy all of these application requirements. Therefore, we report such an elastomer for applications in resorbable synthetic grafts and beyond.

To render good biocompatibility and bioresorbability to the designed elastomer and its degraded components, we selected monomers 1,8-octanediol, glycerol, alkyne-functionalized serinol, sebacic acid, thiomalic acid, and poly(ε-caprolactone)

Received: October 3, 2023
Revised: December 27, 2023
Accepted: December 29, 2023
Published: January 11, 2024

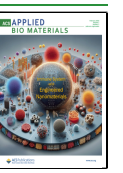

https://doi.org/10.1021/acsabm.3c00894
ACS Appl. Bio Mater. 2024, 7, 863−878

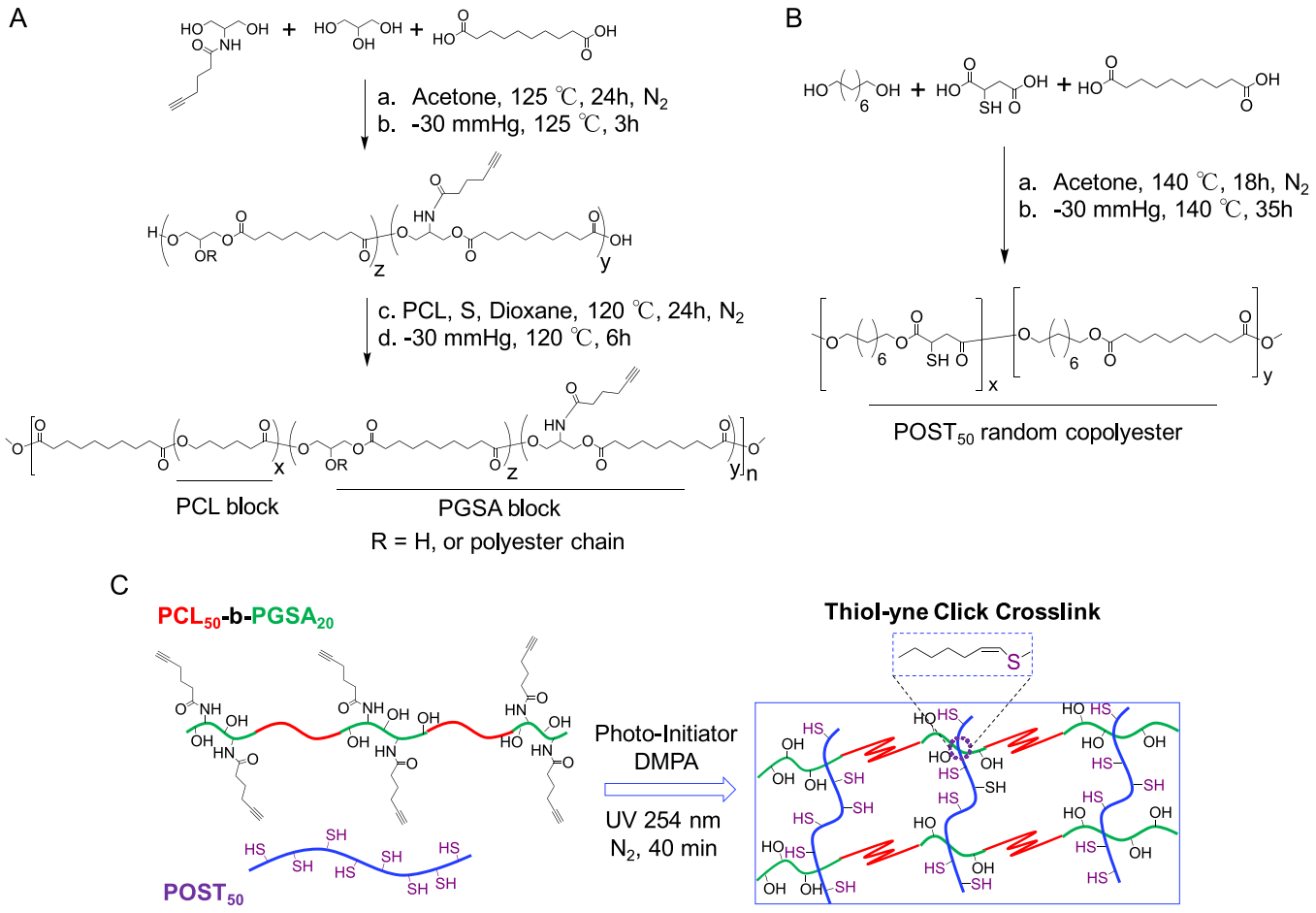

Figure 1. Synthesis routes. (A) Poly(ε-caprolactone)-*b*-poly(glycerol-*co*-sebacate-*co*-alkyne-serinol) block copolyester with the PCL block at 50 mol % and the alkyne pendant at 20 mol % in the PGSA block (PCL_{50}-*b*-$PGSA_{20}$). (B) Poly(1,8-octanediol-*co*-sebacate-*co*-thiomalate) with 50 mol % thiomalate ($POST_{50}$). (C) Schematic illustration of thiol-yne click cross-links between the PCL_{50}-*b*-$PGSA_{20}$ and $POST_{50}$ prepolymers to form network structures. The click cross-link is triggered by UV light at 254 nm in the presence of a photoinitiator (DMPA). The weight ratios of the PCL_{50}-*b*-$PGSA_{20}$ and $POST_{50}$ are used to tune the material properties (e.g., thermal properties, degradation, mechanical properties).

(PCL) as building blocks. Among them, the alkyne-serinol is our recently designed diol monomer to impart alkyne functionalities to polyesters for biomedical applications.[24] Thiomalic acid has been used to make sodium aurothiomalate in the treatment of rheumatoid arthritis.[25] This monomer has also been used to synthesize thiol-bearing polyesters such as poly(1,8-octanediol-*co*-citrate-*co*-thiomalate) and poly(1,8-octanediol-*co*-maleicate-*co*-thiomalate) for biomedical applications.[26] The other monomers such as glycerol, 1,8-octanediol, and sebacic acid have been used to make bioresorbable polyesters of poly(glycerol sebacate) (PGS) and poly(1,8-octanediol citrate) (POC).[27−29] Therefore, these selected monomers can ensure our designed elastomers are biocompatible and bioresorbable.

Prior designs typically combined different monomers into one batch to synthesize a copolyester with a specific composition, which showed limited tunable material properties. If different material properties and performances are required, new syntheses need to be conducted with a different composition by adjusting the monomer ratios, copolymerization with different monomers, or postmodifications.[28,30−32] For example, glycerol, 1,8-octanediol, and sebacic acid at different molar ratios were copolymerized to yield poly(glycerol-*co*-1,8-octanediol-*co*-sebacate) (PGOS) prepolymers, which were thermally cross-linked to form the PGOS elastomers. The material properties such as mechanical properties, hydrophilicity, and degradation rates could be tuned by the prepolymer composition and curing time.[30,32] If the curing time was not included, only synthesis of each prepolymer took about 71 h in the presence of an enzymatic catalyst.[30] In another case, we designed an alkyne-bearing polyester by copolymerizing 1,3-propanediol, alkyne-functionalized serinol, and sebacic acid.[24] This alkyne-bearing random copolyester could be UV-cross-linked with a small dithiol cross-linker in minutes to form elastomers. However, the material properties were also dependent on the prepolymer composition and the cross-linking density. In this case, synthesis of each prepolymer took about 96 h, although the curing was eased by UV-cross-linking.[24] It is worth noting that such a batch-to-batch synthesis of prepolymers with different compositions is time- and energy-consuming.

Here, we use our selected monomers to synthesize a pair of alkyne and thiol-functionalized polyesters to ease the tunability of the material properties and performances for different applications. When the alkyne- and thiol-bearing prepolymers are mixed at different weight ratios, they are quickly cross-linked through thiol-yne click chemistry under UV light to form a series of elastomers. The prepolymer ratios are used to control the material compositions, structures, and properties of the resultant elastomers. These elastomers simultaneously

https://doi.org/10.1021/acsabm.3c00894
ACS Appl. Bio Mater. 2024, 7, 863−878

possess features of robust elasticity, considerable hydrophilicity, and a wide range of tunable degradation and mechanical properties. Further, a mixture of the two prepolymers is electrospinnable and UV-cross-linkable to construct elastic fibrous scaffolds. This report demonstrates the syntheses and characterizations of the prepolymers and the resultant elastomers. We investigate the effects of the chemical structures and compositions on the thermal properties, hydrophilicity, in vitro degradation, elasticity, and mechanical properties. In addition, we also demonstrate the feasibility of fabricating elastic conduits by electrospinning and UV cross-linking as well as examine the relevant mechanical properties of the conduits.

2. RESULTS AND DISCUSSION

2.1. Syntheses of a Pair of Alkyne- and Thiol-Functionalized Polyesters. We have designed a pair of functional polyesters to engineer elastomeric scaffolds for biomedical applications. One polyester is condensed from glycerol, alkyne-functionalized serinol, sebacic acid, and PCL in two steps to form an alkyne-functionalized block copolyester, poly(ε-caprolactone)-*b*-poly(glycerol-*co*-sebacate-*co*-alkyne-serinol) (PCL_x-*b*-$PGSA_y$) (Figure 1A). The alkyne-serinol, glycerol, and sebacic acid are first condensed at a molar ratio of 1:4:5 to make the PGSA block (Figure 1A (step 1) and Table 1). This block bears 20 mol % of alkyne pendants and 80 mol % of unreacted hydroxyl groups. In the second step, the PCL block at 50 mol % based on the PCL repeats to the PGSA repeats is further condensed with the PGSA block to yield the resultant PCL_{50}-*b*-$PGSA_{20}$ block copolyester (Figure 1A (step 2) and Table 1). In this way, the PCL_{50}-*b*-$PGSA_{20}$ prepolymer is designed to combine the soft PGSA block with the relatively stiff PCL block into one system. The PGSA block bears the alkyne pendants for thiol-yne click reactions and the free hydroxyl groups to retain certain hydrophilicity, while the PCL block is to impart crystalline domains. It is worth noting that the initial PCL (M_n = 80 kDa) is reacted with the free hydroxyl groups on the PGSA block through transesterification to form short PCL-*b*-PGSA chains, which are further condensed to form the resultant PCL_{50}-*b*-$PGSA_{20}$ block copolyester, instead of just a diblock structure (Figure 1A (step 2)). Thus, there is no concern about slow degradation of the initial 80 kDa PCL in this prepolymer (Table 1). On the other hand, the PCL blocks are important to impart the crystalline domains that can interact with our designed thiol-bearing polyester based on crystal-domain interactions to make the resultant elastomers as we will demonstrate in the subsequent sections. Previously, the ε-caprolactone monomer was copolymerized with glycerol and sebacic acid to yield a viscous random copolyester of poly(ε-caprolactone-*co*-glycerol-*co*-sebacate), which was dominated by amorphous structure and showed limited tunable material properties.[33] Our PCL_{50}-*b*-$PGSA_{20}$ prepolymer is highly viscoelastic and stretchable because of the soft nature and strong physical interactions between the polymer chains (Figure S2A,B). The PCL_{50}-*b*-$PGSA_{20}$ prepolymer is soluble in acetone, THF, HFIP, DMF, and acetone/DCM cosolvent for use.

Table 1. Monomer Quantities (mmol), Number Average Molecular Weight (M_n), and Polydispersity (PDI) of the as-Made PCL_{50}-b-$PGSA_{20}$ and $POST_{50}$ Prepolymers

sample	PCL:AS:G:S[a], mmol	M_n (Da)/ PDI[b]
PCL_{50}-*b*-$PGSA_{20}$	12.5:5:20:25.0	43,550/5.10
	O:S:T, mmol	
$POST_{50}$	20.0:10.0:10.0	8990/4.15

[a]Poly(ε-caprolactone) (PCL), alkyne-functionalized serinol (AS), glycerol (G), sebacic acid (S), 1,8-octanediol (O), thiomalic acid (T). The PCL quantities are based on its repeat units. The actual moles of each monomer are listed, instead of their molar ratios, given that the current reaction conditions and the tested polymer molecular weight and PDI are related to the current reactant quantities. [b]The polymer molecular weight is tested by gel permeation chromatography (Supporting Information, Figure S3).

The thiol-bearing polyester is condensed from 1,8-octanediol, sebacic acid, and thiomalic acid at a 2:1:1 molar ratio. The polycondensation yields a random copolyester of poly(1,8-octanediol-*co*-sebacate-*co*-thiomalate) with 50 mol % thiomalate ($POST_{50}$) (Figure 1B). The $POST_{50}$ prepolymer appears slightly more solid than a wax (Figure S2C), and is soluble in acetone, DCM, THF, and HFIP, respectively. We would like to note that changes of the monomer fractions, such as the thiomalate in the POST and the alkyne-serinol and PCL block in the PCL-*b*-PGSA, can accordingly alter the prepolymer properties such as the viscoelastic and thermal properties, among others (Data not shown here). Here, we will focus on using the $POST_{50}$ and the PCL_{50}-*b*-$PGSA_{20}$ prepolymers mixing at different weight ratios to make elastomers for investigations (Figure 1C).

2.2. Polymer Molecular Weight and Polydispersity. Gel permeation chromatography (GPC) analysis is used to examine the prepolymer molecular weight and polydispersity (PDI) (Figure S3). The GPC spectrum of the PCL_{50}-*b*-$PGSA_{20}$ prepolymer exhibits a portion of high molecular weight polymers followed by a low molecular weight portion (Figure S3A). The number-average molecular weight (M_n) can reach 43 550 Da with a molar mass distribution (PDI) of 5.10 (Table 1). The relatively high PDI is because the glycerol monomer tends to yield a certain percentage of branched structures.[34] This is a common phenomenon in glycerol-containing polyesters such as the PGS and its derivatives.[31,32] Another reason is because the incorporation of the PCL block increased the viscosity of the reaction system which also contributed to the relatively high molar mass distribution. Nonetheless, incorporation of the PCL block is an efficient strategy to obtain the block copolyester with a relatively high number-average molecular weight (M_n above 43 kDa, Table 1). In contrast, prior glycerol-containing polyesters such as the PGS and its derivatives are difficult to reach an M_n of above 10 kDa, even when using an enzyme catalyst for synthesis.[31,32,34] This is because the glycerol monomer contains three hydroxyl groups that easily form cross-links to achieve a high degree of polymerization. However, it should be noted that the high PDI (5.10) indicates the system still contains a portion of low molecular weight PCL_{50}-*b*-$PGSA_{20}$ prepolymer.

Compared to the PCL_{50}-*b*-$PGSA_{20}$ prepolymer, the $POST_{50}$ shows a relatively low M_n of 8990 Da with a PDI of 4.15 (Table 1 and Figure S3B). Although there is no concern about forming cross-links among the 1,8-octanediol, sebacic acid, and thiomalic acid under the current reaction condition, slight evaporation of the thiomalic acid during the reaction leads to deviation from stoichiometry and thus a relatively low molecular weight. We expect a slightly lower reaction temperature and a longer reaction time in the step shown in Figure 1B(a) might reduce the monomer evaporation and

https://doi.org/10.1021/acsabm.3c00894
ACS Appl. Bio Mater. 2024, 7, 863−878

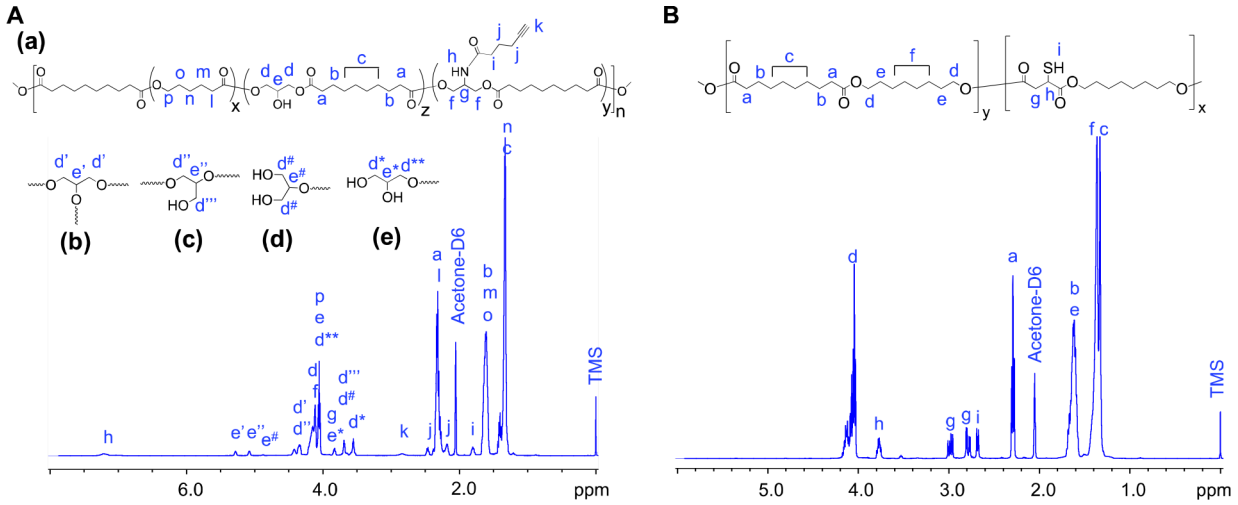

Figure 2. Proton NMR analysis to examine the chemical structures and compositions of the prepolymers. (A) (a) Representative chemical structure of the PCL_{50}-*b*-$PGSA_{20}$ prepolymer. (b) 1,2,3-trisubstituted glycerol to form a branched structure. (c) 1,2 or 2,3-substituted glycerol. (d,e) Portion of glycerol pendent on the chain ends or along the backbone. (B) $POST_{50}$. Each prepolymer demonstrates chemical shifts from each monomer component accordingly, indicating appropriate chemical structures.

increase the molecular weight of the resultant POST prepolymer. Nonetheless, the current $POST_{50}$ can satisfy our application requirements.

2.3. Proton NMR Analysis To Study the Chemical Structure and Composition. Proton NMR analysis is performed to examine the chemical structure and composition of each prepolymer (Figures 2 and S4). The PCL_{50}-*b*-$PGSA_{20}$ sample shows corresponding chemical shifts (δs) from alkyne-serinol, glycerol, sebacate, and PCL block, respectively (Figure 2A). The alkyne-serinol component shows characteristic δs from the methylene protons ($4H_j$ and $2H_i$), alkyne proton (H_k), and amide proton (H_h), which is in agreement with the spectrum of the alkyne-serinol monomer (Figure S1). Because the glycerol bears three hydroxyl groups at 1,2,3-positions for condensation with sebacic acid in a different manner, the δs are relatively complicated. The majority of the reactions occur at the 1,3-position to form a linear structure, showing a δ of methylene protons (H_d) at 4.1141 ppm [Figure 2A(a)]. A small portion of the glycerol reacts with sebacic acid at 1,2,3-, 1,2-, or 2,3-positions, showing δs for the methine proton ($H_{e'}$ and $H_{e''}$) at 5.2795 and 5.0768 ppm, respectively [Figure 2A(b,c)]. Another small portion of the glycerol is pendent along the backbone or on the chain ends, which shows δs for methine proton ($H_e^{\#}$) at 4.8755 ppm, and methylene protons ($H_d^{\#}$ and H_{d*}) at 3.6908 and 3.5530 ppm, respectively [Figure 2A(d,e)]. Such a chemical shift distribution from the glycerol component is similar to previously reported poly(glycerol sebacate).[34] The sebacate component shows three characteristic δs of the methylene protons ($8H_c$, $4H_b$, $4H_a$) at 1.3320, 1.6067, and 2.3183 ppm, respectively. They are overlapped with δs from the PCL methylene protons ($2H_n$, $2H_m$, $2H_o$, $2H_l$). The PCL block also shows a δ of methylene proton ($2H_p$) at 4.0550 ppm.

Compared to the PCL_{50}-*b*-$PGSA_{20}$, the $POST_{50}$ prepolymer is relatively simple in the monomer constituents (Figure 2B). The thiomalate shows δs at 2.6736 ppm for the thiol proton (H_i), 2.7651−2.8105 and 2.9587−3.0114 ppm for the methylene protons ($2H_g$), and 3.7688 ppm for the methine proton (H_h). The sebacate component also demonstrates three characteristic δs at 1.3318, 1.6156, and 2.2926 ppm for the methylene protons ($8H_c$, $4H_b$, and $4H_a$). In this case, the sebacate methylene protons at 1.3318 and 1.6156 ppm are overlapped with the methylene protons ($8H_f$ and $4H_e$) from the 1,8-octanediol component. The 1,8-octanediol component also shows a distinct δ at 4.0594 ppm for the methylene protons ($4H_d$). These proton NMR spectra confirmed the chemical structures of the PCL_{50}-*b*-$PGSA_{20}$ and $POST_{50}$ prepolymers.

Furthermore, we use the proton integration area ratios to identify the actual chemical compositions of the PCL_{50}-*b*-$PGSA_{20}$ and $POST_{50}$ prepolymers (Figure S4 and Table S1). For the $POST_{50}$, the integration area ratio of the protons H_a to H_d is used to determine the sebacate composition to be 51.1 mol % using eq S1. The integration area ratio of H_h to H_d shows the thiomalate content to be 46.9 mol % using eq S2. The actual sebacate to thiomalate molar ratio is about 1.09:1 which is close to their starting ratio at 1:1 in the reaction, indicating an efficient polycondensation of the dicarboxylic acid and 1,8-octanediol monomers to yield the resultant $POST_{50}$ prepolymer. The thiomalate composition is slightly lower than the theoretical value because of a slight evaporation of the thiomalic acid during the reaction process.

For the PCL_{50}-*b*-$PGSA_{20}$ prepolymer, integration area ratios of the proton H_i from alkyne-serinol, H_l, H_m, H_n, and H_o from PCL, and H_a, H_b, and H_c from sebacate are respectively used to calculate the actual compositions of these monomers and PCL repeats according to eqs S3−S5 (Table S1). The actual alkyne-serinol content is slightly lower than the theoretical value because of a slight evaporation of this monomer when making the PGSA block. In contrast, the actual PCL block content is close to the theoretical value because of the difficult evaporation of this building block. Overall, the resultant prepolymers show a desired chemical structure and acceptable actual composition. A slight evaporation of the monomers is not uncommon in a polycondensation reaction that leads to a slight deviation of the actual composition from the theoretical composition.[35] For simplicity, we still use the theoretical contents to designate the prepolymers as $POST_{50}$ and PCL_{50}-*b*-$PGSA_{20}$, respectively.

https://doi.org/10.1021/acsabm.3c00894
ACS Appl. Bio Mater. 2024, 7, 863−878

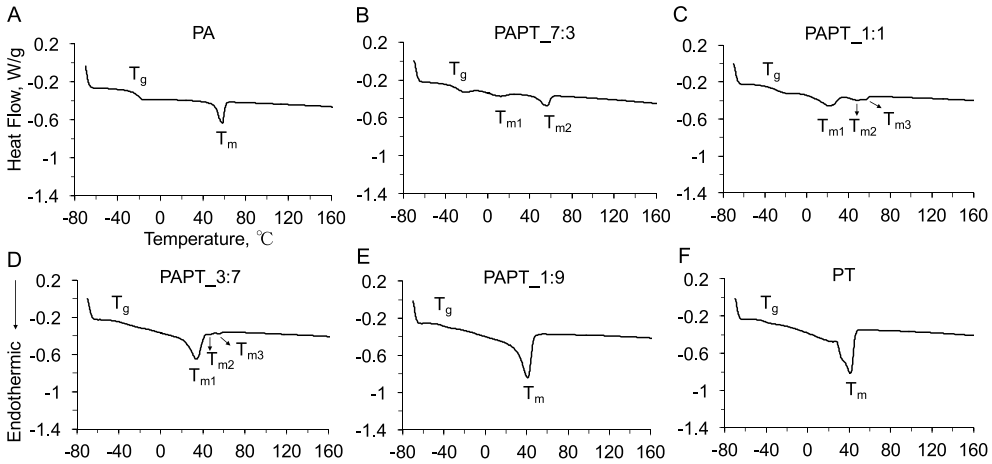

Figure 3. DSC analyses of the PAPT_*x*:*y* elastomers with different PA to PT weight ratios. (A) PA alone. The PCL_{50}-*b*-$PGSA_{20}$ prepolymer is cross-linked with a trithiol cross-linker at 20 mol % cross-links to form the PA alone. (B) PAPT_7:3. (C) PAPT_1:1. (D) PAPT_3:7. (E) PAPT_1:9. (F) PT alone. The $POST_{50}$ is cross-linked with 1,10-decanediol diacrylate at 10 mol % cross-links to form the PT alone.

Table 2. Summary of Glass Transition Temperature (T_g), Melting Temperature (T_m), and Enthalpy (ΔH_m) of the PAPT_x:y Elastomers with PA to PT Weight Ratios (*x*:*y*) Varying from 7:3 to 1:9 and the PA and PT Alone Elastomers (n = 3)[a]

elastomer sample	T_g, °C[b]	T_m, °C	-ΔH_m[c], J/g
PA	−27.4 ± 2.3	58.9 ± 0.9	9.14 ± 0.73
PAPT_7:3	−34.8 ± 0.5	11.4 ± 0.8, 55.7 ± 0.3	7.71 ± 0.48
PAPT_1:1	−36.5 ± 0.4	22.6 ± 0.5, 48.8 ± 0.6, 56.2 ± 0.2	11.6 ± 0.95
PAPT_3:7	−43.1 ± 1.0	34.0 ± 0.6, 47.1 ± 0.4, 54.7 ± 1.1	21.2 ± 0.59
PAPT_1:9	−45.8 ± 0.4	41.1 ± 0.3	35.9 ± 0.61
PT	−45.5 ± 0.1	41.1 ± 0.1	38.5 ± 0.6

[a](a,b) One-way ANOVA was performed for statistical analysis with Bonferroni post-test for multiple pair comparison. [b]T_g: One-way analysis of variance, $p < 0.0001$, ***. For multiple pair comparison, PAPT_7:3 vs PAPT_1:1 and PAPT_3:7 vs PAPT_1:9 vs PT show no significance (ns). Comparison of the other pairs shows a significant difference (***). [c]−ΔH_m: One-way analysis of variance, $p < 0.0001$, ***. For multiple pair comparison, PA vs PAPT_7:3 vs PAPT_1:1 and PAPT_7:3 vs PAPT_1:1 show ns. Comparison of the other pairs shows a significant difference (***). A p value <0.05 is considered significantly different. Data represent the mean value ± standard deviation.

2.4. Thermal Property Studies of the as-Made Prepolymers and Elastomers. We use differential scanning calorimetry (DSC) analysis to examine the thermal properties of the PAPT_*x*:*y* elastomers made from the PCL_{50}-*b*-$PGSA_{20}$ (PA) and $POST_{50}$ (PT) prepolymers at different PA to PT weight ratios (*x*:*y*) (Figures 3 and S5). Glass transition temperature (T_g) is the temperature of the amorphous polymer segments changing from a rigid glassy state to a rubbery state for movements.[36] The melting temperature (T_m) is the temperature of the polymer transitioning from a crystalline state into a viscous flow state, and melting enthalpy (ΔH_m) is proportional to the quantity of the crystalline structures.[36−38]

The DSC data demonstrate that both the PCL_{50}-*b*-$PGSA_{20}$ and $POST_{50}$ prepolymers show T_g and T_m, indicating they are semicrystalline materials at temperatures below the T_m (Figure S5). For the PCL_{50}-*b*-$PGSA_{20}$ prepolymer, the soft PGSA blocks are more amorphous and responsible for the T_g at −39.6 ± 0.03 °C with a weak T_m at −11.6 ± 1.1 °C, whereas the PCL blocks are dominant for the crystalline structures showing two distinct T_ms at 48.3 ± 1.1 °C and 55.0 ± 0.01 °C with an enthalpy of 10.3 ± 0.9 J/g (Figure S5A and Table S2). After the PCL_{50}-*b*-$PGSA_{20}$ prepolymer is cross-linked with a trithiol cross-linker to form the PA-alone elastomer (Figure S6), the PGSA blocks are less flexible to move and difficult to form crystalline structures. As a result, the T_g is elevated to −27.4 ± 2.3 °C and the originally weak T_m at −11.6 ± 1.1 °C is eliminated in the PA alone elastomer (Figure 3A and Table 2). Without interferences from the adjacent soft PGSA blocks, the PCL blocks in the PA alone form crystalline structures showing only one melting temperature (T_m, 58.9 ± 0.9 °C) (Figure 3A), which is similar to that of the 80 kDa PCL control (T_m, 58.2 ± 0.4 °C) (Figure S5C). However, the melting enthalpy (−ΔH_m, 9.14 ± 0.73 J/g) of the PA alone is significantly lower than that of the PCL control (−ΔH_m, 56.1 ± 1.1 J/g) (Figure S5C and Table S2). This is because short PCL blocks are incorporated into the PCL_{50}-*b*-$PGSA_{20}$ polymer backbone and the PCL block content is only 50 mol %, which forms less crystalline domains compared to the 80 kDa PCL control.

The $POST_{50}$ prepolymer shows two T_gs (−50.7 ± 0.7, −16.9 ± 0.7 °C) and one strong T_m at 39.2 ± 0.1°C accompanied by two weak T_ms at 28.2 ± 0.6 and 44.2 ± 0.1 °C, representing a typical random copolymer structure with a semicrystalline nature (Figure S5B and Table S2). The melting enthalpy of the $POST_{50}$ prepolymer (−ΔH_m, 37.8 ± 2.1 J/g) is much higher than that of the PCL_{50}-*b*-$PGSA_{20}$ prepolymer (−ΔH_m, 10.3 ± 0.9 J/g), suggesting the $POST_{50}$ is easier to form crystalline structures. After the $POST_{50}$ is cross-linked with the 1,10-decanediol diacrylate cross-linker to form the PT-alone elastomer, both the T_g and T_m are increased accordingly (Figures 3F and S5B). The phenomenon of increase of the T_g and T_m after cross-linking is similar to the PA alone. Such a phenomenon was also observed in other

https://doi.org/10.1021/acsabm.3c00894
ACS Appl. Bio Mater. 2024, 7, 863−878

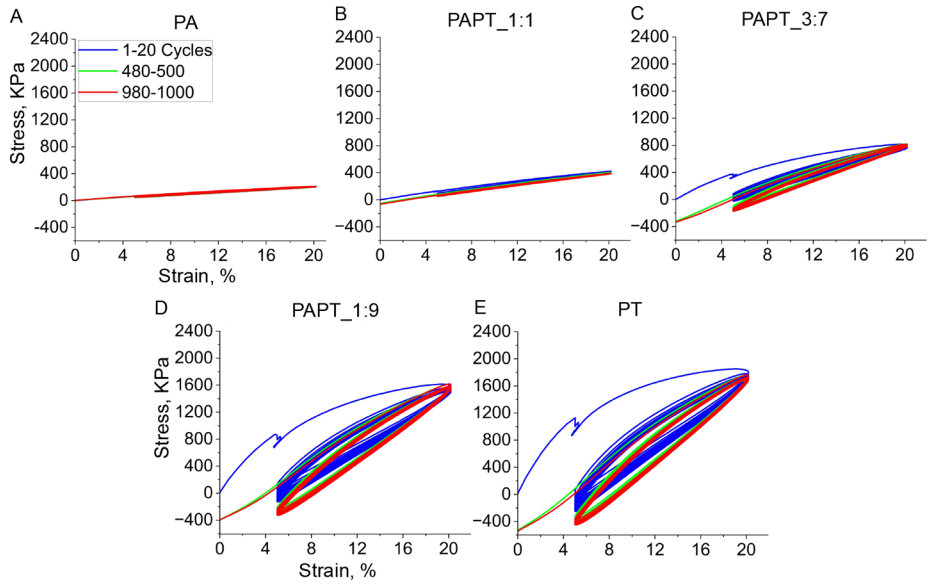

Figure 4. Cyclic tensile tests to evaluate elasticity of the PAPT_*x*:*y* elastomers (n = 3). (A) PA alone. (B) PAPT_1:1. (C) PAPT_3:7. (D) PAPT_1:9. (E) PT alone. When the PA fraction is at 1:1 or above, the elastomers are soft like the PA alone for elastic deformations with a small hysteresis loop, indicating stable networks and robust elasticity. Increase of the PT fraction above 1:1 increases the plastic deformations and network instability.

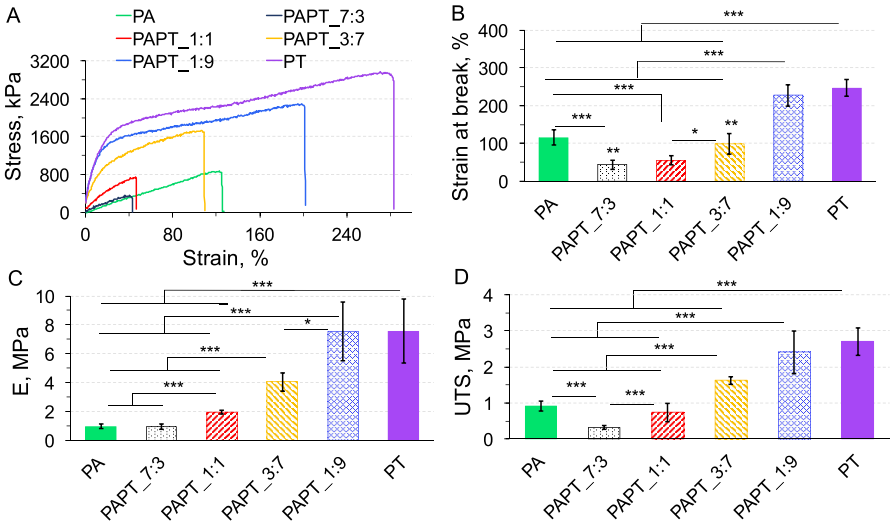

Figure 5. Uniaxial tensile tests of the PAPT elastomers with different PA to PT weight ratios. (A) Representative stress−strain curves. (B) Strain at break, % (p < 0.0001). (C) Elastic modulus (E, MPa) (p < 0.0001). (D) Ultimate tensile strength (UTS, MPa) (p < 0.0001). The cross-links in PAPT_7:3, PAPT_1:1, PAPT_3:7, and PAPT_1:9 are 64, 27, 12, and 3 mol %, respectively. More PT fractions significantly elevate the E and UTS values but increase plastic deformations accordingly due to the formation of more crystal-domain cross-links. *p < 0.05, **p < 0.01, ***p < 0.001. A p-value <0.05 is considered significantly different. Data represent mean value ± standard deviation (SD) (n = 7). (Please note that these elastomer samples were prepared and stored in a 4 °C fridge before the tensile test. The PAPT_1:9 and the PT alone were easier to form crystalline domains than the other samples (Figure 3). The different storage time in the 4 °C fridge likely resulted in the formation of different amounts of crystal-domain cross-links, leading to a relatively large standard deviation in the PAPT_1:9 and the PT alone samples compared to the other elastomer samples.)

copolymer and block copolymer-based elastomers cross-linked with small-molecule cross-linkers.[39,40] In our case, the cross-links make the polymer more compact and the interferences of the soft segments with the crystallization of the stiff segments are inhibited, which likely promoted the crystallization and increased the T_m. On the other hand, the polymer segments between the cross-links are shorter than that of the prepolymer, which hindered the segmental mobility and elevated the T_g.[39]

Different from the PA and PT alone elastomers, the PAPT elastomers show tunable T_g and T_m with the PA to PT weight ratios (Figure 3B−E and Table 2), suggesting that the PA and PT polymer chains can interact with each other to form different amorphous and crystalline structures at the different weight ratios. The T_g is gradually tuned from −34.8 ± 0.5 to −45.8 ± 0.4 °C as the PT fraction increases from 3:7 to 9:1 (Table 2). Interestingly, these PAPT elastomers show new T_ms as the PA to PT ratio changes. For example, the PAPT_7:3 sample shows two T_ms (T_{m1} at 11.4 ± 0.8 °C and T_{m2} at 55.7

https://doi.org/10.1021/acsabm.3c00894
ACS Appl. Bio Mater. 2024, 7, 863−878

± 0.3 °C) (Table 2). The T_{m1} is not observed in either the PA or the PT alone, indicating the formation of new crystalline structures. We deduce that the PT chains interact with the PCL blocks in the PA to form the new crystalline domains. At the same time, the T_{m2} for the PCL crystalline domains is decreased from originally 58.9 ± 0.9 to 55.7 ± 0.3 °C (Figure 3A,B). The enthalpy is slightly reduced too, but not significantly, when comparing the PAPT_7:3 with the PA alone (Table 2). As the PA to PT ratio changes from 7:3 to 1:1 and 3:7, the new melting temperatures (T_{m1}) for the PAPT_1:1 and PAPT_3:7 samples are accordingly increased to 22.6 ± 0.5 and 34.0 ± 0.6 °C, respectively. The enthalpy shows a significant increase too, indicating the formation of more crystalline domains with the increase of the PT fraction (Table 2). At the same time, the PCL crystalline domains are weakened and split into two types of crystalline structures (T_{m2} and T_{m3}) and ultimately disappear in the PAPT_1:9 sample (Figure 3C−E). The PAPT_1:9 possesses a T_g and a T_m similar to the PT alone, but with a significantly lower enthalpy, indicating that the PA chains at this low content can still interact with the PT chains for crystallization.

These DSC studies demonstrate two important findings: (1) the PA and PT polymer chains can interact with each other to form new crystalline structures; (2) the thermal properties (T_g, T_m, and ΔH_m) can be manipulated by the prepolymer ratios in the PAPT elastomers. These thermal properties can be used to control the material properties such as mechanical properties and elasticity to engineer elastomeric scaffolds.[39,40] In addition, we will use the PA and PT mixture for electrospinning to construct PAPT fibrous scaffolds. Strong physical interactions between the PA and PT prepolymers are desirable to form a homogeneous mixture and mediate the solution viscosity for electrospinning to form fibers.[41]

2.5. PCL_{50}-*b*-$PGSA_{20}$ Is Cross-Linked with $POST_{50}$ at Different Weight Ratios To Form Elastomers with a Wide Range of Tunable Properties. We examined the elasticity and mechanical properties of the PAPT elastomers with PA to PT weight ratios varying from 7:3 to 1:9 using cyclic tensile and uniaxial tensile tests (Figures 4 and 5). The PA and PT alone elastomers were also compared. These PAPT elastomers are the same as those for the DSC studies (Figure 3). In this way, we can establish the relationship of the mechanical properties with the thermal properties.

All of these PAPT elastomers can undergo elastic deformations within 20% strain for at least 1000 cycles without a break, but the hysteresis loops are different among them (Figure 4). The PAPT_1:1 elastomer is soft and shows a small hysteresis loop, indicating a robust elasticity like the PA alone (Figure 4A,B). As the PT fraction increases, the hysteresis loops increase proportionally, indicating less stable networks (Figure 4C−E). This is because more PT fractions in the elastomers form more crystalline domains as physical cross-links (crystal-domain cross-links).[42] The DSC studies have indicated that these crystal-domain cross-links are formed by the interactions between the PA and PT chains and are proportional to the PT fraction (Figure 3). The more crystal-domain cross-links result in increased plastic deformations and network instability because some of the crystal-domain cross-links are damaged and cannot recover quickly under the current cyclic loading rate (30 mm/min). The cyclic tensile curves show an increased extent of fracture between 4 and 6% strain in the first cycle as the PT fraction increases (Figure 4). These data suggest that the PAPT elastomers with the PA fraction at 1:1 or above are soft and more likely to form coiled chains between the cross-links for reversible deformations with better elasticity.

After knowing the elastic performance, we then examined the mechanical properties of these PAPT elastomers. The mechanical properties are synergistically affected by the PA to PT ratios, the polymer chain structures (e.g., coiled chains, crystalline) between the cross-links, and the cross-linking densities. We would like to note that the PA prepolymer bears alkyne pendants of ∼420 μmol/g, and the PT prepolymer bears thiol groups of ∼1530 μmol/g according to the proton NMR analysis (Table S1). When the PA and PT are mixed at 7:3, 1:1, 3:7, and 1:9 weight ratios to make these elastomers, their cross-linking densities are varied from 64%, 27%, 12%, to 3% by mole, respectively. We assumed all of the alkyne groups were fully reacted with the thiol groups at a 1:1 molar ratio by 40 min UV cross-linking. In principle, one mole of the alkyne group can react with two moles of thiol groups.[24,43] Although the thiol groups are excessive to the alkyne groups in our case, we still make such an assumption because the thiol groups are pendent on the PT backbone that is difficult to move for further reactions once the PT chains are cross-linked with the PA chains. Using PAPT_1:1 as an example, we compared the effects of UV cross-linking time at 1, 4, and 40 min on the mechanical properties (Figure S7). The PAPT with 4 min cross-linking shows nearly the same strain at break, *E*, and UTS as the sample with 40 min cross-linking, indicating they are cross-linked similarly. In contrast, 1 min cross-linking forms a slightly more stretchable elastomer with a significantly higher *E* and UTS compared to the other two samples. This is because less covalent cross-links are formed by 1 min cross-linking, leading to longer polymer chains between the cross-links and thus the formation of more crystalline domains. The more crystal-domain cross-links contribute to elevating the *E* and UTS values significantly but also impart more plastic deformations in the PAPT_1 min sample (Figure S7). In addition, we also examined the elasticity of the PAPT_1:1 elastomers cross-linked for 4 and 40 min (Figure S8). Both the elastomers show similar elastic deformation profiles with small hysteresis loops without a break, indicating a similarly stable network. These data indicate that 4 min UV exposure is sufficient to accomplish a full thiol-yne click cross-link like the one with 40 min cross-linking. The data also confirmed our assumption that the thiol-yne click cross-link is dominated by a 1:1 molar ratio for reaction. 40 min UV exposure is adopted to ensure a complete click cross-link even at a lower alkyne concentration as the PA fraction decreases.[43] Therefore, the following PAPT elastomers with different PA-to-PT ratios were cross-linked for 40 min for comparison (Figure 5).

Notably, the *E* values can be tuned from 0.96 ± 0.18 MPa for the PAPT_7:3 to 7.5 ± 2.0 MPa for the PAPT_1:9. At the same time, the strain at break increases from 43 ± 11 to 227 ± 28%, and the UTS is accordingly increased from 0.31 ± 0.050 to 2.4 ± 0.59 MPa as the PA to PT ratio changes from 7:3 to 1:9. The tunability is easily achieved by adjusting the PA to PT ratios to make these elastomers. Intriguingly, the *E*, UTS, and strain at the break of these PAPT elastomers are all proportional to the PT fraction (Figure 5). As we know that increase in the PT fraction results in a decrease of the cross-linking densities. In other word, the *E*, UTS, and strain at break are all increased as the cross-linking density decreases. This is different with conventional thermoset elastomers, which typically show an *E* proportional to the cross-links but the

https://doi.org/10.1021/acsabm.3c00894
ACS Appl. Bio Mater. 2024, 7, 863−878

strain at break is inverse to the cross-links.[32,44] In our case, the PA to PT ratios can simultaneously affect the cross-linking densities and the polymer chain structures (crystalline vs coiled chains). The higher PT fraction leads to a decrease in the cross-linking densities, longer polymer segments between the cross-links, and thus, the more stretchable PAPT elastomers (Figure 5B). At the same time, the longer polymer segments between the cross-links can form more crystal-domain cross-links that elevate the *E* and UTS (Figure 5C,D). We would like to note that the crystalline structures are different at the different PA to PT ratios as demonstrated by the DSC analysis (Figure 3). When the PA to PT ratios are at 7:3 and 1:1, these two PAPT elastomers undergo nearly a linear elongation (Figure 5A). The linear elongation suggests these two elastomers are dominated by coiled chains for elastic deformations at room temperature or above. Most of the crystal-domain cross-links in the PAPT_1:1 are reversible to dissipate the stress that helps maintain a stable network structure as demonstrated by the cyclic tensile tests (Figure 4A,B).

As the PT fraction is further increased from 1:1 to 9:1 in the PAPT elastomers, the covalent cross-links are reduced from 27 to 3 mol %. The more PT fractions impart more crystal-domain cross-links that dominate the cross-links. This is evidenced by the increased plastic deformations and hysteresis loops in the elastic deformations (Figures 4C−E and 5A). The presence of a plastic deformation region (about 16−40% strain) gradually transitions the elongation from a high-modulus region to a low-modulus region until break (Figure 5A). The high-modulus elongation is controlled by both the covalent and the crystal-domain cross-links, whereas the low-modulus elongation is determined by the covalent cross-links because most of the crystal-domain cross-links have been dissociated by stretching above 40% strain. Indeed, the crystal-domain cross-links can significantly increase the *E* value with relatively low covalent cross-links and make the elastomers more stretchable to reach a significantly higher UTS (Figure 5B,D). However, too many crystal-domain cross-links lead to less stable network structures that are not desired for some applications. This is particularly true for elastomeric scaffolds such as synthetic grafts for in situ remodeling in a mechanically dynamic environment. These scaffolds typically require relatively consistent mechanical performances and dimensions across the remodeling process.[5,45]

Based on the above analyses, the PA to PT weight ratios at 7:3 to 1:1 show a reasonable range to make PAPT elastomeric scaffolds for soft tissue engineering applications with the *E* tuned between 0.96 ± 0.18 and 2.0 ± 0.14 MPa. Although the elastomers show a relatively low strain at the break between 43 and 55% (Figure 5B), this strain range is still suitable for most soft tissues such as ligaments and arteries because their deformations are typically within 20% strain.[46] In addition, benefiting from the easy formation of crystalline structures between the PA and PT chains serving as physical cross-links, our PAPT elastomers can simultaneously increase the *E*, UTS, and strain at break as the PT fraction increases (Figures 3 and 5). The previously designed photocurable polyesters such as the (meth)acrylated PGS might be able to tune the mechanical properties like our PAPT elastomers by cross-linking with macromolecular cross-linkers such as diacrylated PCL and diacrylated PEG.[47] However, the presence of these slow-degrading macromolecule chains might compromise the resorbability of the resultant scaffold and induce complications such as chronic inflammatory response, calcification, and inhibition of tissue regeneration for applications in the resorbable grafts.[23,48]

2.6. Studies on Hydrophilicity and In Vitro Degradation of the Elastomers. Not only the tunable mechanical properties but also appropriate hydrophilicity and tunable degradation rate are important to design medical devices for different tissues given their different host responses and regenerative speeds.[6,8] In the current design, these PAPT elastomers possess considerable amounts of free hydrophilic hydroxyl and thiol groups and show water contact angles between 78.3 ± 3.56 and 85.6 ± 3.58 degrees as the PA to PT weight ratio varies from 7:3 to 1:9 (Figure S9). Typically, a material with a water contact angle of less than 90 degrees is considered to be hydrophilic.[10] In our case, an elastomer with a water contact angle of less than 85 degrees appears suitable for applications in the resorbable grafts according to our prior studies. For example, a palmitate-modified PGS elastomer with a water contact angle of ∼84 degrees could allow an efficient infiltration of host cells in the graft walls for remodeling in a rat carotid artery model.[31] Compared with the palmitate-modified PGS elastomer and the graft,[5,31] the water contact angle measurements indicate these PAPT elastomers appear to possess an appropriate hydrophilicity for the resorbable grafts.

Although the hydrophilicity is close among these elastomers, their degradation profiles are significantly different as examined by an accelerated degradation test in a 60 mM NaOH solution at 37 °C (Figure 6). The accelerated degradation test is adopted because it can quickly distinguish different degradation profiles of these elastomers. In addition, we previously used the same method to examine the in vitro degradation behaviors of the PGS and its derivatives.[31,49] In combination with the in vivo degradation of the PGS-based elastomers,[5,50] we can estimate the likely in vivo degradation of these PAPT elastomers.

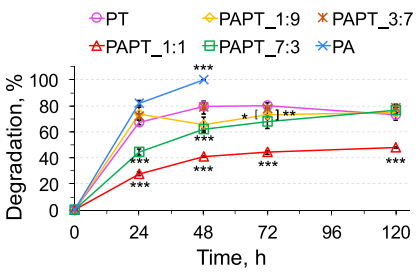

Figure 6. Accelerated degradation tests of the PAPT elastomers, the PA alone, and the PT alone in a 60 mM NaOH solution at 37 °C. When the PA to PT ratio is at 7:3 to 1:1, these two PAPT elastomers show relatively steady degradation profiles dominated by a surface erosion fashion. The PAPT_1:1 degradation is about 1.6 times slower than that of the PAPT_7:3 sample. Statistical analysis for the PAPT_1:1 sample versus the other samples: $p < 0.0001$ (24−120 h). $^{*}p < 0.05$, $^{**}p < 0.01$, $^{***}p < 0.001$. A p value < 0.05 is considered significantly different. Data represent mean value ± standard deviation (SD) ($n = 3$).

The in vitro degradation tests indicate that the degradation behaviors of the PAPT elastomers are also tunable by the PA to PT weight ratios (Figure 6). The PA alone is fully degraded within 48 h at a relatively steady rate dominated by a surface erosion fashion like the PGS-based elastomers.[31,49] In contrast, the PT alone shows a quick degradation in the first 24 h, followed by a plateau of slow degradation, exhibiting a bulk

https://doi.org/10.1021/acsabm.3c00894
ACS Appl. Bio Mater. 2024, 7, 863−878

erosion fashion (Figure 6). The PT polymer backbone is composed of relatively hydrophilic 1,8-octanediol-thiomalate segments for quick degradation and hydrophobic 1,8-octanediol-sebacate segments for slow degradation. Because the PT chains are easy to form crystalline structures (Figure 3), the PT alone sample forms a relatively loose structure with more micropores as noted during the sample preparation process. The more micropores will allow water molecules to penetrate throughout the networks. As a result, the PT alone undergoes bulk erosion with two distinct degradation behaviors at the early and the later stages. We stopped the in vitro degradation test at 120 h because the samples via bulk erosion were prone to break into small pieces and particles. Some of them were easily washed away during the sample collection process and thus compromised the accuracy of the degradation test.

Because of the different degradation features of the PA and the PT alone, their mixtures at the different ratios can, therefore, efficiently mediate the degradation profiles of the resultant PAPT elastomers. When the PA to PT ratio is at 7:3 and 1:1, these two PAPT elastomers are dominated by surface erosion. This is manifested by a relatively steady degradation rate (Figure 6), and the sample remains a disc shape but gradually becomes thinner across the experimental time (Figure S10B), indicating the degradation mainly occurs on the sample surfaces. The PAPT_7:3 elastomer is softer with 64 mol % cross-links compared to the PAPT_1:1 with 27 mol % cross-links (Figure 5). Theoretically, the former with more cross-links should be slower in degradation than the latter. However, the degradation of the PAPT_7:3 sample is about 1.6 times that of the PAPT_1:1 sample. This is because the PAPT_7:3 sample possesses 20 wt % more PA than that of the PAPT_1:1 sample. Thus, more hydroxyl groups are present on the networks. The more hydroxyls absorb more water molecules through hydrogen bonding interactions to facilitate the degradation of the PAPT_7:3 sample. We would like to note that the hydroxyl pendants on the polyester backbone are important to mediate the polyester degradation. For comparison, the PCL backbone does not bear hydroxyl pendants. As a result, the PCL control shows a negligible degradation over 120 h under the same testing condition (Figure S10A), even though the water contact angle of the PCL control is close to the PAPT elastomers (Figure S9A). It is worth noting that the free thiol groups on the PT backbone can also facilitate the degradation at the early stage but are less effective than the hydroxyl groups as shown in the PA alone (Figure 6). As the PT fraction is further increased from 1:1 to 9:1, the PAPT elastomers are dominated by bulk erosion with degradation profiles like the PT alone (Figure 6). This is because of the reduction of the covalent cross-links, formation of relatively loose network structures, and increase of the crystalline domains and micropores like the phenomena observed in the PT alone sample.

For some applications, surface erosion-dominated elastomer is preferred to regulate the degradation and mechanical properties in a relatively steady manner.[51] Thus, the mechanical properties and elasticity can be maintained at a relatively consistent level as the elastomer is gradually degraded.[47] Our PAPT elastomers with PA to PT weight ratios between 7:3 and 1:1 appear to satisfy these application requirements. The in vitro degradation rates of the PAPT_7:3 and the PAPT_1:1 elastomers are about 5−9 times slower than that of an acrylated PGS elastomer under the same testing condition.[49] A PGS porous conduit is degraded in about 2−4 weeks in a rat carotid artery model.[5] Therefore, we speculate that a PAPT porous conduit would likely last for 2−9 months in the same rat model by adjusting the PA to PT weight ratios between 7:3 and 1:1. Of course, implantation of different materials will induce different host responses, different levels of reactive oxygen species and hydrolytic enzymes as well as different cell infiltration and growth in the scaffolds, among others.[52] All these factors will affect the in vivo degradation. Our in vitro degradation data in comparison with the PGS degradation can only provide an estimation for in vivo use. More studies need to be conducted to understand the host responses and biodegradation of the PAPT elastomers.

2.7. In Vitro Cytocompatibility. The cytocompatibility is evaluated by culturing NIH/3T3 fibroblast cells on the PAPT_1:1 coating over 48 h. Resazurin assay is used to evaluate the impacts of the elastomer on cell viability.[53] After 24 and 48 h incubation, the cellular metabolic capacity of the PAPT sample can reach 80 ± 4.7 and 88 ± 8.7% relative to the TCPS control, respectively (Figure 7). Although the cell metabolic capacity of the PAPT sample is significantly lower than that of the TCPS control, the normalized value above 85% at 48 h indicates a cytocompatible nature of the material. According to the cell morphologies (Figure S11), the fibroblast cells can adhere to the PAPT coating similar to those on the TCPS control. However, the cells appear to be slightly less spread on the PAPT surface compared to the TCPS control after 24 h incubation (Figure S11A,B). This phenomenon suggests that the fibroblast cells grow slightly slower on the PAPT surface than on the TCPS. This is likely because the PAPT surface is slightly more hydrophobic than the TCPS surface, instead of the cytotoxicity of the material. We observed a similar phenomenon in a prior study that a more hydrophobic elastomer could slow down endothelial cell growth on the elastomer surface.[31] Here, we selected the PAPT_1:1 elastomer as a representative for the cytocompatibility study as this formulation contains an equal amount of the PA and PT prepolymers. The other formulations with different PA-to-PT ratios might show a slightly different cell adhesion and growth rate, but the cytocompatibility will not be a concern.

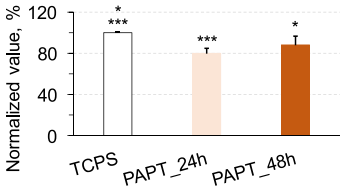

Figure 7. Resazurin assay to evaluate cell viability of NIH/3T3 cells on the PAPT_1:1 elastomer. After 48 h incubation, the normalized value of the cellular metabolism on the PAPT sample is 88 ± 8.7% relative to the TCPS control, indicating a good cytocompatibility of the elastomer. One-way ANOVA analysis with Bonferroni's multiple comparison test is performed for statistical analyses. $p = 0.0005$. A $p < 0.05$ is considered significantly different. The data represent mean value ± SD ($n = 5$).

2.8. PCL_{50}-*b*-$PGSA_{20}$ and $POST_{50}$ Prepolymer Mixture Is Electrospinnable and UV-Cross-Linkable To Construct Elastic Fibrous Conduits. Electrospinning is a mature method to construct resorbable grafts for evaluation in different animal models.[23] We therefore use the PA and PT

https://doi.org/10.1021/acsabm.3c00894
ACS Appl. Bio Mater. 2024, 7, 863−878

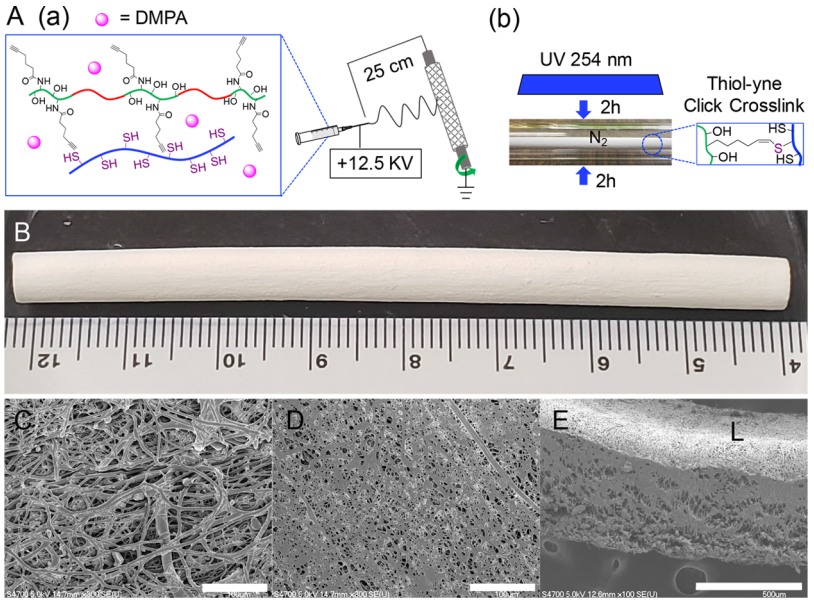

Figure 8. (A) (a) Illustration of electrospinning. A mixture of the PA and PT prepolymers at 1:1 weight ratio with 10 mol % of DMPA photoinitiator is loaded in a syringe for electrospinning. (b) UV cross-linking of the PAPT conduit. The electrospun conduit is inserted into a glass tube and exposed under UV light for click cross-linking to form an elastic fibrous conduit. (B) Photograph of the electrospun PAPT conduit with a length of about 8.2 cm. The conduit inner diameter is 4.76 mm that is controlled by the rotating stainless steel mandrel used as the fiber collector. (C–E) Representative morphologies of the PAPT conduit by SEM observation. (C) Outer surface, (D) luminal surface, and (E) cross-section. Scale bar: C, D, 100 μm; E, 500 μm. Luminal space is labeled as L.

prepolymers at a 1:1 weight ratio as an example to make an electrospun PAPT conduit, followed by UV cross-linking to yield an elastic fibrous conduit (Figure 8). Under the current electrospinning condition, there are small amounts of microparticles sprayed and distributed along with the fibrous networks (Figure 8A,C). The fibers are partially fused at the overlap areas including the interconnection areas because of the soft and somehow viscous nature of the PA and PT mixture before UV cross-linking. Not surprisingly, the luminal surface which is in direct contact with the mandrel surface is also partially fused under the stress from the outer layers (Figure 8D). According to prior studies of PCL-based grafts, a relatively flat luminal surface could improve hemocompatibility and endothelialization, and thus inhibit thrombogenicity.[48] Therefore, our PAPT conduit with a relatively flat luminal surface might possess a similar performance, which is beneficial for graft remodeling. Please note that the current UV cross-linking condition can cure the fibers close to the outer surface (Figure 8A(b)). Below 50–100 μm from the outer surface, the SEM image shows a flattened interface on the conduit cross-section caused by the cutting process (Figure 8E), indicating that these fibers are yet to be fully cross-linked. Here, we only preliminarily examined the electrospinnability and UV cross-linkability using the PA and PT prepolymers to fabricate the fibrous conduits. Further optimization of the electrospinning and UV cross-linking conditions is underway to control the graft parameters such as the fiber diameter, pore size, porosity, wall thickness, and mechanical properties. These parameters are important for graft remodeling in vivo.[23]

In addition, we examined the mechanical properties of the PAPT conduit fabricated under the current condition (Figure 9). The mechanical properties of the longitudinal (PAPT_L) and circumferential (PAPT_C) directions under dry and wet conditions are compared. Both the PAPT_L and PAPT_C show nearly a linear elongation until break (Figure 9A). For

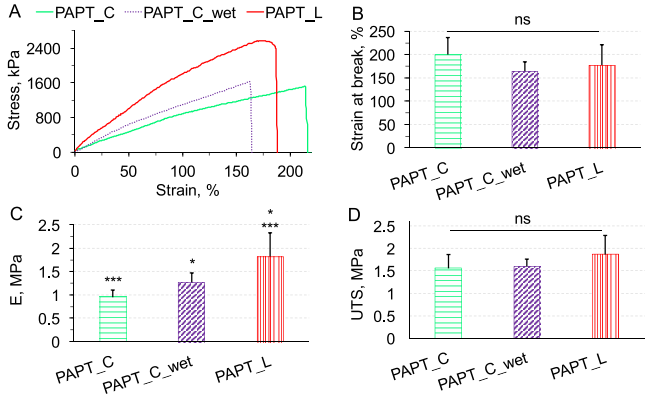

Figure 9. Mechanical properties of the electrospun PAPT fibrous conduit under dry and wet conditions. (A) Representative stress–strain curves at longitudinal (PAPT_L) and circumferential (PAPT_C) directions under dry and wet conditions. (B) Strain at break (%), p = 0.1561. (C) Elastic modulus (E, MPa), p = 0.0003. (D) Ultimate tensile strength (UTS, MPa), p = 0.1598. One-way ANOVA analysis with Bonferroni's multiple comparison test is performed for statistical analysis. *p < 0.05, ***p < 0.001. A p value < 0.05 is considered significantly different. Data represent mean value ± standard deviation (SD) (n = 7).

the dry conduit, the strain at break can reach 200 ± 36% circumferentially and 177 ± 44% longitudinally without a significant difference (Figure 9B). The conduit is much more stretchable than the PAPT_1:1 bulk elastomer likely because the conduit is a porous structure, and the cross-linking densities are low under the current UV cross-linking condition. Interestingly, the circumferential E (0.95 ± 0.16 MPa) is significantly lower than the longitudinal E (1.8 ± 0.51 MPa) (Figure 9C). We have yet to know the exact reason. The UTS can reach 1.6 ± 0.30 MPa circumferentially and 1.9 ± 0.42 MPa longitudinally without a significant difference (Figure

https://doi.org/10.1021/acsabm.3c00894
ACS Appl. Bio Mater. 2024, 7, 863–878

9D). To compare the conduit dimension and mechanical properties under a hydrated condition, the conduit was immersed in PBS solution (1×, pH 7.4) and incubated at 37 °C for 48 h to reach an equilibrium state. The conduit dimension remains consistent before and after the incubation (Figure S12). The circumferential E of the wet conduit increases to 1.3 ± 0.20 MPa but shows a nonsignificant difference compared to that of the dry conduit (0.95 ± 0.16 MPa). The UTS and strain at the break of the wet conduit remain similar to those of the dry conduit. A slight increase of the circumferential E is likely caused by the infiltration of the PBS salt into the fiber microstructures, which possibly affects the crystalline structures of the PAPT fibers by incubation at 37 °C for a tested period. Nonetheless, the close circumferential mechanical properties of the dry and wet conduits suggest a stable tubular structure for applications in a biological setting. It is worth noting that the circumferential mechanical properties are close to that of a rat aorta circumferentially (Strain at break: 215 ± 18.9%, E: 0.94 ± 0.080 MPa, and UTS: 2.0 ± 0.17 MPa),[54] suggesting that our PAPT conduit would be sufficiently strong to withstand blood pressure after implantation. It should be noted that the graft mechanical properties can be further tuned by adjusting the PA-to-PT ratios (e.g., 7:3 to 1:1), the fiber diameters, and the UV cross-linking conditions. Although the current PAPT conduit is yet to be an optimized version for in vivo studies, the low circumferential E, high UTS, and high stretchability are a good sign for the PAPT conduit to be sutured and mechanically match the native rat aorta for reversible elastic deformations along with blood pulsation for remodeling.[15,54]

Prior designs of resorbable grafts mainly use polyesters such as poly(lactic acid) (PLA), poly(glycolic acid) (PGA), poly(lactic-*co*-glycolic acid) (PLGA), poly(ε-caprolactone) (PCL), and poly(lactic-*co*-caprolactone) (PLCL), among others.[22] These polyesters not only possess attractive characteristics such as mechanical strength, biocompatibility, and biodegradability but also show limitations. The grafts made from these polyesters are typically rigid, hydrophobic, and slow in degradation.[55−58] Cells are difficult to infiltrate and proliferate in these graft walls to produce extracellular matrices (ECM) and form ECM alignments to fully remodel the synthetic grafts.[59−61] Biodegradable polyurethane (PU) elastomer has also been used to engineer resorbable grafts.[18,62] Although the PU grafts could be designed to possess an elastic modulus (0.21−0.27 MPa) and compliance close to the rat carotid artery, too slow degradation of the PU elastomer also impeded the graft remodeling.[18] Like those rigid polyester grafts, cells were difficult to infiltrate and proliferate in the PU graft wall to fully remodel it in a rat carotid artery model.[18] Interestingly, a composite graft comprised a porous PGS conduit stabilized with a thin layer of fibrous PCL sheath possessed a suitable elastic modulus (~0.42 MPa), robust elasticity, and suitable hydrophilicity that could be nearly fully remodeled in months in both the rat carotid and aortic artery models.[63−65] However, too quick degradation of the PGS core led to immature remodeling, dilation, and split in 10−16 days in an ovine carotid model.[14] A following study improved the graft design by modifying the PGS with hydrophobic palmitates to make the elastomer softer and inhibit graft degradation by about 1.3 times in vitro.[31] As a result, the remodeling outcomes were improved accordingly to generate a new blood vessel with a structure and performance closer to the native rat carotid artery.[5] However, we noted that the presence of the slow-degrading PCL sheath hindered tissue integration between the media and adventitia layers in the remodeled grafts.[5] Further, the postmodification of the PGS with the palmitates showed a limited inhibition of the degradation. In addition, the PGS-based grafts were made by a salt-leaching method that was difficult to scale up for large animal studies.[5,63] Based on these prior studies, we speculate that the appropriate elastic modulus, robust elasticity, and suitable hydrophilicity and degradation rate likely play synergistic roles in graft remodeling. Our PAPT elastomers with the PA to PT weight ratios between 7:3 and 1:1 appear to simultaneously possess features of appropriate hydrophilicity and degradation rate, robust elasticity, and suitable mechanical properties for the resorbable grafts. More importantly, the electrospinnability and UV-cross-linkability make the PAPT elastomer feasible to scale up the grafts for large animal studies in the future. In this way, we can fabricate the entire grafts using the PAPT elastomer with no need of either a carrying polymer for electrospinning or a slow-degrading polymer sheath (e.g., PCL sheath) for stabilization. It should be noted that the suitability of our designed PAPT elastomers and the electrospun conduits for resorbable grafts is speculated based on our in vitro data compared with the prior resorbable grafts such as the PGS, the palmitate-functionalized PGS, and the PCL grafts, among others.[5,6,48,63,65] We will further optimize the electrospinning conditions to construct the PAPT conduits and evaluate in a rat abdominal aorta model to understand the host responses and the graft remodeling outcomes in the next step.

3. CONCLUSIONS

We have reported a strategy to ease the control of the material structure and properties by designing a pair of alkyne- and thiol-functionalized polyesters for biomedical applications. The mixture of the prepolymer pair at different weight ratios can be quickly UV-cross-linked through thiol-yne click chemistry to generate a series of biodegradable elastomers. These elastomers show a wide range of tunable material properties (e.g., thermal properties, mechanical properties, and degradation rate) with a robust elasticity. These tunable features are important to design scaffolds for different tissue engineering applications given their different host responses, mechanical properties, and regenerative abilities. The elastomers with elastic moduli tuned between 0.96 and 7.5 MPa are likely suitable for both soft and some hard tissues. One of our main objectives is to use the prepolymers to fabricate a bioresorbable graft by electrospinning and UV-cross-linking methods. Our in vitro data have demonstrated that the elastomers are cytocompatible, and the electrospun conduit could simultaneously possess features of appropriate hydrophilicity and degradation rate, robust elasticity, and suitable mechanical properties. Further optimization of the electrospinning and UV-cross-linking conditions is underway to control the graft parameters. Although we designed the PAPT elastomers particularly for the resorbable grafts, these elastomers might be useful for other tissue engineering applications as well.

4. EXPERIMENTAL SECTION

4.1. Chemicals. Alkyne-serinol monomer was synthesized according to our reported protocol with a slight modification (Supporting Information, Figure S1).[24] Sebacic acid was recrystallized in ethanol two times, and 1,8-octanediol (≥98%, BeanTown

https://doi.org/10.1021/acsabm.3c00894
ACS Appl. Bio Mater. 2024, 7, 863−878

Chemical) was recrystallized in acetone once before use. All other chemicals such as glycerol (HPLC grade, Alfa Aesar), thiomalic acid (≥99.0% (HPLC), Sigma-Aldrich), trimethylolpropane tris(3-mercaptopropionate) (TMPMP, ≥95.0%, Sigma-Aldrich), 1,10-bis(acryloyloxy)decane (90%, Sigma-Aldrich), 2,2-dimethoxy-2-phenylacetophenone (DMPA, >98.0%, TCI), (poly(ε-caprolactone) (PCL, M_n = 80 000 Da, Sigma-Aldrich), acetone-D_6 (99.9%, contains 0.03% v/v TMS, Sigma-Aldrich), acetone (ACS grade, VWR BDH CHEMICALS), 1,1,1,3,3,3-hexafluoro-isopropanol (HFIP, ≥99%, Sigma-Aldrich), and 1,4-dioxane anhydrous (99.8%, Alfa Aesar) were used as received. The acetone was dried with molecular sieves (3 Å) for at least 20 h before use. The 1,4-dioxane anhydrous was stored in a desiccator with drierite.

4.2. Synthesis of Poly(ε-caprolactone)-*block*-poly(glycerol-*co*-sebacate-*co*-alkyne-serinol). Block copolyesters of poly(ε-caprolactone)-*b*-poly(glycerol-*co*-sebacate-*co*-alkyne-serinol) (PCL_x-*b*-$PGSA_y$) with 50 mol % PCL and 20 mol % alkyne-serinol were synthesized in two steps. In the first step, 20 mol % of alkyne-serinol relative to sebacic acid was mixed with glycerol and sebacic acid for polycondensation to yield the $PGSA_{20}$ block (Table 1). Specifically, 5.00 mmol alkyne-serinol (0.926 g), 20.0 mmol glycerol (1.842 g), 25.0 mmol sebacic acid (5.056 g), and 5 mL acetone were mixed in a 100-ml three-neck round-bottom flask. The reaction flask was connected with a Schlenk line and a nitrogen outlet flask. The reaction was set in an oil bath on a magnetic stirrer hot plate. The reactants were gently purged with nitrogen gas for at least 15 min at room temperature and then heated at 125 °C to completely dissolve the reactants by magnetically stirring under a nitrogen atmosphere for 2 h. The reaction was remained at 125 °C for 24 h with a gentle nitrogen purge through the reaction solution, followed by further condensation at 125 °C for 3 h under a vacuum condition (30 mmHg vacuum) to yield the $PGSA_{20}$ block. The reaction was cooled down to room temperature for the second step.

In the second step, 1.425 g of 80 kDa PCL (12.5 mmol, based on the moles of the PCL repeats), 51 mg of sebacic acid (0.25 mmol), and 5 mL of 1,4-dioxane anhydrous were added to mix with the $PGSA_{20}$. The mixture was purged with nitrogen gas for at least 15 min at room temperature, and then vigorously stirred at 120 °C for 2 h under a nitrogen atmosphere to dissolve the PCL and uniformly mix with the PGSA block. The reaction was remained at 120 °C for 24 h with a gentle nitrogen purge through the reaction solution, followed by vacuum condensation (30 mmHg vacuum) for 6 h to yield the resultant PCL_{50}-*b*-$PGSA_{20}$ copolyester. The product was then transferred into a centrifuge tube and stored in −20 °C fridge for use.

4.3. Synthesis of Poly(1,8-octanediol-*co*-sebacate-*co*-thiomalate) Copolyester. The poly(1,8-octanediol-*co*-sebacate-*co*-thiomalate) (POST) was condensed from 1,8-octanediol, sebacic acid, and thiomalic acid at a molar ratio of 2:1:1. Specifically, 20.0 mmol 1,8-octanediol (2.925 g), 10.0 mmol sebacic acid (2.022 g), 10.0 mmol thiomalic acid (1.502 g), and 5 mL of acetone were charged in the three-neck round-bottom flask. The reactants were gently stirred and purged with nitrogen gas for 30 min at room temperature. The condensation was remained at 140 °C for 18 h with a gentle nitrogen purge through the reaction solution, followed by vacuum condensation (30 mmHg vacuum) for 35 h to yield the resultant prepolymer with 50 mol % of thiomalate ($POST_{50}$).

4.4. Material Characterizations. Proton NMR analysis (500 MHz, Bruker) was performed to examine the chemical structure and composition of the resultant PCL_{50}-*b*-$PGSA_{20}$ and $POST_{50}$ prepolymers. Approximately 15 mg of each prepolymer was dissolved in 0.75 mL of acetone-D_6 for test.

DSC analysis (Mettler Toledo 823E, Polymer Differential Scanning Calorimeter) was performed to examine the thermal properties. Each sample with a mass between 5.00 and 10.00 mg was prepared and loaded in a standard Tzero pan with a lip for the DSC analysis. The test was performed from −70 to 200 °C with a heating rate at 10 °C/min. The nitrogen flow rate was set at 60 mL/min for the purge furnace chamber and 200 mL/min for dry gas flow, respectively. Each sample was scanned two times and the second scan was adopted for analysis. Each elastomer sample was replicated three times (n = 3). The prepolymers and the 80 kDa PCL control were replicated two times (n = 2).

The molecular weight of the PCL_{50}-*b*-$PGSA_{20}$ prepolymer was analyzed using a size exclusion chromatography instrument (SHIMADZU HPLC Nexera Series) connected with a sample injection port, a degas system, a column oven, and three detectors. One precolumn (Shodex OHpak LB-G 6B, ID 8.00 × 50.00 mm) and one column (Shodex OHpak LB-803, ID 8.00 × 300.00 mm) were set as the stationary phase. N,N-dimethylformamide (DMF, HPLC grade) was used as the mobile phase. The detection system was equipped with a UV detector (SPD-40), a RI detector (RID-20A), and a multiple angle light scattering detector (WYATT, miniDAWN). ASTRA software (Version 8.1.2.1) was used for molecular weight analysis. Poly(styrene) standard (M_n /PDI, 30 kDa/1.02) at 5.00 mg/mL was used for calibration. The sample solution was prepared in DMF at 5.00−10.00 mg/mL by incubating at 45 °C overnight in an incubator and then orbital-shaking for 1 h at room temperature for test. DMF flow rate was set at 0.500 mL/min. The column oven temperature was set at 40 °C, and the detection temperature was set at room temperature. 20.0 μL of each solution was injected for test.

4.5. Preparation of the PA Alone and PT Alone Elastomer. A trithiol molecule, trimethylolpropane tris(3-mercaptopropionate) (TMPMP), was used as a small-molecule cross-linker to cross-link the PCL_{50}-*b*-$PGSA_{20}$ (PA) prepolymer via UV triggered thiol-yne click chemistry to make the PA alone elastomer. According to the actual alkyne content in the prepolymer (Table S1), the alkyne-to-thiol molar ratio was set at 1:1 for cross-linking to form 20 mol % cross-links. Specifically, 3.6 g of the prepolymer (containing approximately 1.50 mmol alkyne pendants) was dissolved in 12.0 mL of acetone in a glass vial by rotatory agitation at room temperature for about 48 h, followed by gently swirling in a water bath at 45 °C for about 5 min to yield a clear 30% wt/v prepolymer solution. To a round-bottom flask, 200 mg of TMPMP cross-linker (0.50 mmol), 54 mg of DMPA UV initiator (0.21 mmol, 14% relative to the moles of the thiol groups), and the prepolymer solution were subsequently added and mixed for about 10 min by magnetically stirring with a gentle nitrogen purge through the solution. The mixture was respectively transferred into six rectangular silicone molds in a glovebox. Each mold (50 × 15 × 2.5 mm^3) was clamped between two glass slides. Each side of the mold was exposed under UV light at 254 nm for 20 min (total 40 min exposure) to yield six pieces of the PCL_{50}-*b*-$PGSA_{20}$ gel. The polyester gel samples were subsequently washed in acetone/deionized water (1:1, v/v) for 48 h and deionized water for 72 h. The washing solution was replaced every 24 h. The washed PCL_{50}-*b*-$PGSA_{20}$ samples were freeze-dried and then further dried at 60 °C overnight in a vacuum oven (30 mmHg vacuum). The dried samples were compact translucent sheets for characterizations.

To prepare the PT alone elastomer, a 30% wt/v $POST_{50}$ solution was prepared in 12.0 mL of acetone by rotatory agitation overnight at room temperature. Then, 83 mg of 1,10-bis(acryloyloxy)decane (290 μmol, 5 mol % relative to the thiol groups) and 15 mg of DMPA (60 μmol, 10 mol % relative to the acrylate groups) were mixed with the $POST_{50}$ prepolymer solution by UV exposure for 40 min to make the PT alone sample with 10 mol % cross-links. All of the other procedures were the same.

4.6. UV Cross-Link To Make PCL_{50}-*b*-$PGSA_{20}$/$POST_{50}$ Elastomers at Different Weight Ratios. The PCL_{50}-*b*-$PGSA_{20}$ (PA) prepolymer (~420 μmol alkyne/g) was cross-linked with the $POST_{50}$ (PT) prepolymer (~1530 μmol thiol/g) to yield various PAPT elastomers. The sample names were designated as PAPT_*x*:*y*, where the *x*:*y* represents the PA-to-PT weight ratios. We prepared PAPT_7:3, PAPT_1:1, PAPT_3:7, and PAPT_1:9 for comparison.

Using PAPT_1:1 as an example, 1.80 g of PCL_{50}-*b*-$PGSA_{20}$ (containing 756 μmol alkyne groups) and 1.80 g of $POST_{50}$ (containing 2754 μmol thiol groups) were respectively dissolved in 6.0 mL of acetone at room temperature by rotatory agitation overnight, followed by gently swirling in a water bath at 45 °C for ~5 min to form two clear 30% wt/v prepolymer solutions. After cooling to room temperature, 27 mg of DMPA UV initiator (110 μmol, 15 mol % relative to the moles of the alkyne groups) and the two

https://doi.org/10.1021/acsabm.3c00894
ACS Appl. Bio Mater. 2024, 7, 863−878

prepolymer solutions were subsequently added to a round-bottom flask, and mixed for about 10 min by magnetically stirring with a gentle nitrogen gas purge through the solution. The mixed prepolymer solution was then transferred into six rectangular silicone molds for UV cross-linking in the glovebox. All of the other procedures, including the UV exposure time (20 min each side), the sample washing, freeze-drying, and heat-drying processes, were the same as the preparation of the PA elastomer. In addition, we also prepared the PAPT_1:1 samples with UV cross-linking for 1 and 4 min (0.5 and 2 min UV exposure each side), respectively. These samples were designated as PAPT_1 min and PAPT_4 min. They were used to compare with the PAPT_40 min to examine the effects of the cross-linking time on the elastomer properties.

A PCL (M_n = 80,000 Da) sheet with a thickness of 1.0 mm was made and used as a control. The PCL platelets were loaded in a rectangular silicone mold (a silicone sheet mounted on an aluminum sheet) and compressed at 150 °C under 400 P.S.I. for 1 h using a hot press (WABASH Hydraulic Press).

4.7. Preparation of the Elastomer Coatings and Water Contact Angle Measurements. Each of the above prepared prepolymer/cross-linker/DMPA solutions was used to prepare elastomer coatings by casting about 1 mL of each solution on a glass slide, followed by UV cross-linking for 0.5, 2, or 20 min in the glovebox. A PCL (M_n = 80,000 Da) coating was also prepared by casting a 15% wt/v PCL in DCM solution on a glass slide and evaporated in a fume hood overnight. These coatings were further dried at 60 °C overnight in a vacuum oven (30 mmHg Vacuum). These coating samples were used for water contact angle measurements to compare the hydrophilicity of these elastomers.

Water contact angle measurement was performed by the sessile drop method using Ossila Contact Angle Goniometer equipped with Ossila Contact Angle v3.1.2.2 software (Ossila Ltd., UK). Ten μL of deionized water was dropped on each coating surface. The water contact angle at 10 s after dropping was recorded for comparison (n = 7).

4.8. In Vitro Degradation Test. An accelerated degradation was conducted in a 60 mM NaOH solution at 37 °C to examine the degradation kinetics of these elastomers (n = 3). Disc samples were punched from the as-made elastomer sheets with a diameter of 6 mm and thickness of about 1.0 mm using a circular puncher. Disc samples from the PCL sheet were also prepared as a control. The initial mass (M_0) of each sample was recorded. Then, 5.0 mL of 60 mM NaOH solution was added to each sample, followed by incubating at 37 °C for 6, 12, 18, 24, 48, 74, and 120 h, respectively. At each time point, the residual samples were collected, washed with deionized water three times, and dried at 70 °C under reduced pressure (30 mmHg vacuum) for 24 h. The residual mass (M_r) for each sample was recorded. The degradation rate was calculated as degradation % = $(M_0 - M_r)/M_0 \times 100\%$.

4.9. Mechanical Property Tests. Strip samples (25 × 2 × 1 mm) were cut from these elastomer sheets with a neck length set at 11 mm for tests. Cyclic tensile tests (n = 3) were performed to evaluate the elasticity for reversible deformations with an elongation rate set at 30 mm/min and a strain range between 5 and 20% using Bose ElectroForce 3200 Series III Test Instrument with a 5 LB-Force loading cell (Bose Corporation, Minnesota, USA). A uniaxial tensile test (n = 7) was conducted to compare the mechanical properties with an elongation rate at 10 mm/min using MTS Acumen Electrodynamic Test System with a 3 kN loading cell (MTS Systems Corporation, MN, USA). Because of the limited sensitivity of this MTS instrument, 11 data points were averaged to smooth the stress–strain curve for calculation of the Young's modulus (E), ultimate tensile strength (UTS), and strain at break for each sample.

4.10. In Vitro Cytocompatibility Study. The 30% wt/v of PAPT_1:1 prepolymer mixture containing 10 mol % DMPA photoinitiators in acetone solution (see the Section 4.6) was diluted to 3% wt/v by acetone. Then, 20 μL of the diluted prepolymer solution was evenly spread on a 12 mm round cover glass and air-dried in a fume hood for 30 min. The prepolymer coating was UV-cross-linked at 254 nm in a glovebox for 2 min to form PAPT_1:1 coating. The coating was dried in a vacuum oven at 60 °C overnight. The coating samples were then washed in ethanol for 48 h to remove the photo-initiator residues, and the ethanol was replaced every 24 h. The washed coating was then dried in the vacuum oven (28 mmHg vacuum) at 60 °C overnight for use.

An in vitro cytotoxicity assay was performed by culturing NIH/3T3 fibroblast cells on the PAPT_1:1 coating according to the standard protocol (ISO 10993). The 3T3 cells (passage 6) were cultured in Dulbecco's modified eagle's medium (DMEM, ATCC, Catalog# 30-2002) containing 10% of fetal bovine serum (FBS, Fisherbrand Research grade, Canadian Sourced, Catalog# FB12999102) and 1% of Gibco penicillin–streptomycin (10,000 U/mL, Catalog# 15-140-122) at 37 °C with 5% CO_2 for 3 days until sufficient quantities were obtained. The cells were detached, washed, and resuspended in the cell media at 3.8×10^5 cell ml^{-1} for use.

Each PAPT_1:1 coated slide was placed on a circular hydrophobic parafilm in a six-well plate with the coating layer orientated upward and sterilized by UV exposure for 10 min in a biological hood (n = 5). To each coated slide, 100 μL of the cell suspension (3.8×10^4 cells) were seeded on the coating surface. Additional 4 drops of the cell media (50 μL/drop) were added to the parafilm to surround the coating sample to prevent the cell media from evaporation. To a 24-well plate, 100 μL of the same cell suspension was seeded in each well as a TCPS control (n = 5). In addition, the PAPT_1:1 coated slide was placed in each well and incubated with the cell media alone as a blank control to examine if the resazurin agent would be reduced by the PAPT coating alone or not (n = 5). The cell-seeded PAPT coating, the PAPT blank control, and the TCPS control were incubated in an incubator at 37 °C with 5% CO_2 overnight (~20 h). The overnight incubation ensured that the cells adhered and grew on the coating surface, which was compared with the TCPS control under the same culturing condition. The cell-seeded coating samples were then transferred from the 6-well plate to the nonseeded wells of the 24-well plate. The cell media were replaced with 500 μL of fresh cell media for further incubation. After an additional 24 and 48 h incubation, the Resazurin Cell Viability Assay Kit (Biotium Inc., CA, USA) was used to examine the cellular viability according to the manufacturer's instructions. Briefly, the resazurin agent and the cell media were mixed at 1:10 v/v to form a working solution. Then the cell media were removed and 400 μL of the resazurin working solution was added to each well, followed by incubating at 37 °C for 4 h in the incubator. 100 μL of the incubated resazurin assay solution was transferred to a 96-well plate with 3 replicates for each well. The colorimetric absorbance was recorded using a microplate reader (Ao Microplate Reader AC3000, Azure Biosystems, CA, USA) at 570 and 600 nm, respectively. The live cells were proportional to the absorbance of the resazurin solution at 570 nm. The cell viability was compared based on a normalized value of the PAPT_1:1 coating relative to the TCPS control using the below equation according to the manufacturer's instruction.

$$\text{Normalized value, } \% = \frac{(O_2 \times A_1) - (O_1 \times A_2)}{(O_2 \times P_1) - (O_1 \times P_2)} \times 100$$

where O_1 was a molar extinction coefficient (E) of oxidized resazurin at 570 nm and equal to 80,586; O_2 was the E of oxidized resazurin at 600 nm and equal to 117,216. A_1 and A_2 were the absorbance values of the testing wells at 570 and 600 nm; P_1 and P_2 were the absorbance values of the TCPS control wells at 570 and 600 nm, respectively.

4.11. Electrospinning to Construct Fibrous Conduits. An amount of 0.45 g of PCL_{50}-b-$PGSA_{20}$ prepolymer and 0.45 g of $POST_{50}$ prepolymer were, respectively, dissolved in a cosolvent of 0.60 mL of acetone and 0.90 mL of dichloromethane (DCM) (2:3, v/v) by rotatory agitation overnight at room temperature to yield two 30% wt/v prepolymer solutions. The two prepolymer solutions were then combined and 4.5 mg DMPA UV initiator (10 mol % relative to alkyne groups) was added. The solution was mixed by vortexing for 1 min and rotatory agitation for 10 min at room temperature. The mixed prepolymer solution was loaded in a 3-ml syringe with a 22 G blunt needle (3.8 cm in length). The syringe was then set on a syringe

https://doi.org/10.1021/acsabm.3c00894
ACS Appl. Bio Mater. 2024, 7, 863–878

pump (NE-1000, Pump Systems Inc., USA) with a flow rate set at 13.4 μL/min. The needle was connected with a positive voltage at +12.5 kV (GLASSMAN HIGH VOLTAGE, Inc., Series EL). A stainless-steel mandrel with a 4.76 mm diameter was set in a horizontal level to the needle tip, and connected with the ground. The mandrel was already coated with a thin layer of PEO (5M Da) using a 1% PEO in deionized water solution and dried overnight at room temperature. The distance between the needle tip to the mandrel was 25 cm. The mandrel rotating rate was set at 100 rpm. The electrospun PAPT fibers were then collected on the rotating mandrel. After the electrospinning was completed, the mandrel with the collected fibrous tube was inserted into a glass tube and two ends were sealed. The glass tube was purged with nitrogen gas for about 15 min and then exposed to UV light (254 nm) for 2 h. The tube was rotated 180 degrees and exposed for another 2 h. The UV cross-linked fibrous tube was then immersed in ethanol/deionized water (50% v/v) for about 24 h. The fibrous tube was gently detached from the mandrel, further washed in deionized water for 48 h, and freeze-dried for tests. The luminal surface, outer surface, and cross-section of the fibrous tube were observed by SEM imaging. A 1.5 cm tube was cut for a longitudinal tensile test, and a 0.5 cm tube was cut for a circumferential tensile test (n = 7). Another set of 0.5 cm tubes was immersed in 5.0 mL of PBS (1×, pH 7.4) and incubated at 37 °C for 48 h (n = 7). After cooling down to room temperature for 4 h, tensile tests were performed to examine the circumferential mechanical properties of these wet tubes to compare with those of the dry tubes.

4.12. Statistical Analysis. Statistical analysis was performed using one-way ANOVA analysis with a posthoc Bonferroni's multiple comparison test. A p value < 0.05 is considered significantly different. Data represented mean value ± standard deviation (SD).

■ ASSOCIATED CONTENT

Supporting Information

The Supporting Information is available free of charge at https://pubs.acs.org/doi/10.1021/acsabm.3c00894.

Additional data include (1) synthesis and characterization of alkyne-serinol monomer; (2) viscoelastic property and photographic images of the prepolymers; (3) molecular weight analysis of the prepolymers; (4) proton NMR analysis of the PCL_{50}-b-$PGSA_{20}$ and $POST_{50}$ prepolymers; (5) DSC analyses of the PCL_{50}-b-$PGSA_{20}$ and $POST_{50}$ prepolymers; (6) illustration of the PCL_{50}-b-$PGSA_{20}$ prepolymer cross-linked with a trithiol cross-linker; (7) effects of UV-cross-linking time on the mechanical properties of the PAPT_1:1 elastomers; (8) comparison of hydrophilicity of the PAPT elastomers by water contact angle measurements; (9) in vitro degradation of the PAPT elastomers with different cross-linking times; (10) fibroblast cell morphologies on the PAPT elastomer and the TCPS surfaces; and (11) comparison of the PAPT tubular dimension by incubating in PBS at 37 °C for 48 h (PDF)

■ AUTHOR INFORMATION

Corresponding Author

Xiaochu Ding − *Health Research Institute, Michigan Technological University, Houghton, Michigan 49931, United States; Department of Chemistry, Michigan Technological University, Houghton, Michigan 49931, United States;* orcid.org/0000-0001-7908-7329; Phone: +1-(906) 487-2865; Email: xding@mtu.edu

Authors

Zhongtian Zhang − *Department of Biomedical Engineering, Michigan Technological University, Houghton, Michigan 49931, United States*

Christopher Kluka − *Department of Materials Science and Engineering, Michigan Technological University, Houghton, Michigan 49931, United States*

Saad Asim − *Department of Biomedical Engineering, Michigan Technological University, Houghton, Michigan 49931, United States*

James Manuel − *Department of Biomedical Engineering, Michigan Technological University, Houghton, Michigan 49931, United States*

Bruce P. Lee − *Department of Biomedical Engineering, Michigan Technological University, Houghton, Michigan 49931, United States;* orcid.org/0000-0002-6529-0032

Jingfeng Jiang − *Health Research Institute, Michigan Technological University, Houghton, Michigan 49931, United States; Department of Biomedical Engineering, Michigan Technological University, Houghton, Michigan 49931, United States*

Patricia A. Heiden − *Department of Chemistry, Michigan Technological University, Houghton, Michigan 49931, United States*

Caryn L. Heldt − *Health Research Institute, Michigan Technological University, Houghton, Michigan 49931, United States; Department of Chemical Engineering, Michigan Technological University, Houghton, Michigan 49931, United States;* orcid.org/0000-0002-0776-8763

Muhammad Rizwan − *Department of Biomedical Engineering, Michigan Technological University, Houghton, Michigan 49931, United States;* orcid.org/0000-0001-6192-0036

Complete contact information is available at: https://pubs.acs.org/10.1021/acsabm.3c00894

Notes

The authors declare the following competing financial interest(s): A provisional patent, entitled Photo-crosslinkable, biodegradable elastomers and resorbable synthetic grafts, was filed on 06/23/2023 by the Michigan Technological University (Application #: 63/510,057).

■ ACKNOWLEDGMENTS

The research in this work is supported by the National Heart, Lung, And Blood Institute and the National Institute of General Medical Sciences of the National Institutes of Health under Award Numbers R15HL159602 (XD) and R15GM135875 (BPL), the Office of Naval Research under Award Number N00014-20-1-2230 (BPL), and the Portage Health Foundation and Research Excellence Fund (XD) of the Michigan Technological University. The GPC system for the polymer molecular weight analysis was purchased through the Office of Naval Research-DURIP Award (N00014-21-1-2877). Drs. Kathryn Perrine and Parya Siahcheshm at the Michigan Technological University Department of Chemistry helped train the DSC analysis. Ms. Fatemeh Razaviamri at the Michigan Technological University Department of Biomedical Engineering provided help with the cytocompatibility assay. We also would like to thank Dr. Yadong Wang, Dr. Ying Chen, and Mr. Yifan Ma at Cornell University for their efforts in the polymer molecular weight analysis.

REFERENCES

(1) Ye, H.; Zhang, K.; Kai, D.; Li, Z.; Loh, X. J. Polyester elastomers for soft tissue engineering. *Chem. Soc. Rev.* **2018**, *47* (12), 4545−4580.
(2) Rai, R.; Tallawi, M.; Grigore, A.; Boccaccini, A. R. Synthesis, properties and biomedical applications of poly(glycerol sebacate) (PGS): A review. *Prog. Polym. Sci.* **2012**, *37* (8), 1051−1078.
(3) Mendibil, X.; Gonzalez-Perez, F.; Bazan, X.; Diez-Ahedo, R.; Quintana, I.; Rodriguez, F. J.; Basnett, P.; Nigmatullin, R.; Lukasiewicz, B.; Roy, I.; Taylor, C. S.; Glen, A.; Claeyssens, F.; Haycock, J. W.; Schaafsma, W.; Gonzalez, E.; Castro, B.; Duffy, P.; Merino, S. Bioresorbable and Mechanically Optimized Nerve Guidance Conduit Based on a Naturally Derived Medium Chain Length Polyhydroxyalkanoate and Poly(epsilon-Caprolactone) Blend. *ACS Biomater Sci. Eng.* **2021**, *7* (2), 672−689.
(4) Fujimoto, K. L.; Yamawaki-Ogata, A.; Uto, K.; Usui, A.; Narita, Y.; Ebara, M. Long term efficacy and fate of a right ventricular outflow tract replacement using an elastomeric cardiac patch consisting of caprolactone and D L-lactide copolymers. *Acta biomaterialia* **2021**, *123*, 222−229.
(5) Fu, J.; Ding, X.; Stowell, C. E. T.; Wu, Y. L.; Wang, Y. Slow degrading poly(glycerol sebacate) derivatives improve vascular graft remodeling in a rat carotid artery interposition model. *Biomaterials* **2020**, *257*, No. 120251.
(6) Fukunishi, T.; Ong, C. S.; Yesantharao, P.; Best, C. A.; Yi, T.; Zhang, H.; Mattson, G.; Boktor, J.; Nelson, K.; Shinoka, T.; Breuer, C. K.; Johnson, J.; Hibino, N. Different degradation rates of nanofiber vascular grafts in small and large animal models. *Journal of Tissue Engineering and Regenerative Medicine* **2020**, *14* (2), 203−214.
(7) Fang, S.; Ellman, D. G.; Andersen, D. C. Review: Tissue Engineering of Small-Diameter Vascular Grafts and Their In Vivo Evaluation in Large Animals and Humans. *Cells* **2021**, *10* (3), 713.
(8) Iismaa, S. E.; Kaidonis, X.; Nicks, A. M.; Bogush, N.; Kikuchi, K.; Naqvi, N.; Harvey, R. P.; Husain, A.; Graham, R. M. Comparative regenerative mechanisms across different mammalian tissues. *NPJ. Regen Med.* **2018**, *3*, 6.
(9) Niemczyk-Soczynska, B.; Gradys, A.; Sajkiewicz, P. Hydrophilic Surface Functionalization of Electrospun Nanofibrous Scaffolds in Tissue Engineering. *Polymers* **2020**, *12* (11), 2636.
(10) Law, K.-Y. Water−surface interactions and definitions for hydrophilicity, hydrophobicity and superhydrophobicity. *Pure Appl. Chem.* **2015**, *87* (8), 759−765.
(11) Jeong, S. I.; Kwon, J. H.; Lim, J. I.; Cho, S. W.; Jung, Y.; Sung, W. J.; Kim, S. H.; Kim, Y. H.; Lee, Y. M.; Kim, B. S.; Choi, C. Y.; Kim, S. J. Mechano-active tissue engineering of vascular smooth muscle using pulsatile perfusion bioreactors and elastic PLCL scaffolds. *Biomaterials* **2005**, *26* (12), 1405−1411.
(12) Coenen, A. M. J.; Bernaerts, K. V.; Harings, J. A. W.; Jockenhoevel, S.; Ghazanfari, S. Elastic materials for tissue engineering applications: Natural, synthetic, and hybrid polymers. *Acta biomaterialia* **2018**, *79*, 60−82.
(13) Hashizume, R.; Hong, Y.; Takanari, K.; Fujimoto, K. L.; Tobita, K.; Wagner, W. R. The effect of polymer degradation time on functional outcomes of temporary elastic patch support in ischemic cardiomyopathy. *Biomaterials* **2013**, *34* (30), 7353−7363.
(14) Stowell, C. E. T.; Li, X.; Matsunaga, M. H.; Cockreham, C. B.; Kelly, K. M.; Cheetham, J.; Tzeng, E.; Wang, Y. Resorbable vascular grafts show rapid cellularization and degradation in the ovine carotid. *J. Tissue Eng. Regener. Med.* **2020**, *14*, 1673−1684.
(15) Zhen, L.; Creason, S. A.; Simonovsky, F. I.; Snyder, J. M.; Lindhartsen, S. L.; Mecwan, M. M.; Johnson, B. W.; Himmelfarb, J.; Ratner, B. D. Precision-porous polyurethane elastomers engineered for application in pro-healing vascular grafts: Synthesis, fabrication and detailed biocompatibility assessment. *Biomaterials* **2021**, *279*, No. 121174.
(16) Kennedy, K. M.; Bhaw-Luximon, A.; Jhurry, D. Cell-matrix mechanical interaction in electrospun polymeric scaffolds for tissue engineering: Implications for scaffold design and performance. *Acta biomaterialia* **2017**, *50*, 41−55.
(17) Carnicer-Lombarte, A.; Chen, S. T.; Malliaras, G. G.; Barone, D. G. Foreign Body Reaction to Implanted Biomaterials and Its Impact in Nerve Neuroprosthetics. *Front Bioeng Biotechnol* **2021**, *9*, No. 622524.
(18) Stahl, A.; Hao, D.; Barrera, J.; Henn, D.; Lin, S.; Moeinzadeh, S.; Kim, S.; Maloney, W.; Gurtner, G.; Wang, A.; Yang, Y. P. A bioactive compliant vascular graft modulates macrophage polarization and maintains patency with robust vascular remodeling. *Bioact Mater.* **2023**, *19*, 167−178.
(19) Shojaee, M.; Bashur, C. A. Compositions Including Synthetic and Natural Blends for Integration and Structural Integrity: Engineered for Different Vascular Graft Applications. *Adv. Healthcare Mater.* **2017**, *6* (12), No. 1700001.
(20) Radke, D.; Jia, W.; Sharma, D.; Fena, K.; Wang, G.; Goldman, J.; Zhao, F. Tissue Engineering at the Blood-Contacting Surface: A Review of Challenges and Strategies in Vascular Graft Development. *Adv. Healthcare Mater.* **2018**, *7* (15), No. 1701461.
(21) Liu, R. H.; Ong, C. S.; Fukunishi, T.; Ong, K.; Hibino, N. Review of Vascular Graft Studies in Large Animal Models. *Tissue Engineering Part B: Reviews* **2018**, *24* (2), 133−143.
(22) Stowell, C. E. T.; Wang, Y. Quickening: Translational design of resorbable synthetic vascular grafts. *Biomaterials* **2018**, *173*, 71−86.
(23) Rocco, K. A.; Maxfield, M. W.; Best, C. A.; Dean, E. W.; Breuer, C. K. In Vivo Applications of Electrospun Tissue-Engineered Vascular Grafts: A Review. *Tissue Engineering Part B: Reviews* **2014**, *20* (6), 628−640.
(24) Ma, W.; Ding, X.; Chen, Y.; Wang, Y. Synthesis and Characterization of Alkyne-Functionalized Photo-Cross-Linkable Polyesters. *ACS Omega* **2022**, *7* (18), 15540−15546.
(25) Rau, R.; Herborn, G.; Menninger, H.; Blechschmidt. Comparison of intramuscular methotrexate and gold sodium thiomalate in the treatment of early erosive rheumatoid arthritis: 12 month data of a double-blind parallel study of 174 patients. *British Journal of Rheumatology* **1997**, *36*, 345−352.
(26) Yapor, J. P.; Neufeld, B. H.; Tapia, J. B.; Reynolds, M. M. Biodegradable crosslinked polyesters derived from thiomalic acid and S-nitrosothiol analogues for nitric oxide release. *J. Mater. Chem. B* **2018**, *6* (24), 4071−4081.
(27) Wang, Y.; Ameer, G. A.; Sheppard, B. J.; Langer, R. A tough biodegradable elastomer. *Nat. Biotechnol.* **2002**, *20*, 602−606.
(28) Yang, J.; Webb, A. R.; Pickerill, S. J.; Hageman, G.; Ameer, G. A. Synthesis and evaluation of poly(diol citrate) biodegradable elastomers. *Biomaterials* **2006**, *27* (9), 1889−1898.
(29) Yang, J.; Webb, A. R.; Ameer, G. A. Novel Citric Acid-Based Biodegradable Elastomers for Tissue Engineering. *Adv. Mater.* **2004**, *16* (6), 511−516.
(30) Lang, K.; Bhattacharya, S.; Ning, Z.; Sánchez-Leija, R. J.; Bramson, M. T. K.; Centore, R.; Corr, D. T.; Linhardt, R. J.; Gross, R. A. Enzymatic Polymerization of Poly(glycerol-1,8-octanediol-sebacate): Versatile Poly(glycerol sebacate) Analogues that Form Monocomponent Biodegradable Fiber Scaffolds. *Biomacromolecules* **2020**, *21* (8), 3197−3206.
(31) Ding, X.; Chen, Y.; Chao, C. A.; Wu, Y. L.; Wang, Y. Control the Mechanical Properties and Degradation of Poly(Glycerol Sebacate) by Substitution of the Hydroxyl Groups with Palmitates. *Macromol. Biosci.* **2020**, *20*, No. 2000101.
(32) Lang, K.; Quichocho, H. B.; Black, S. P.; Bramson, M. T. K.; Linhardt, R. J.; Corr, D. T.; Gross, R. A. Lipase-Catalyzed Poly(glycerol-1,8-octanediol-sebacate): Biomaterial Engineering by Combining Compositional and Crosslinking Variables. *Biomacromolecules* **2022**, *23* (5), 2150−2159.
(33) Rostamian, M.; Kalaee, M. R.; Dehkordi, S. R.; Panahi-Sarmad, M.; Tirgar, M.; Goodarzi, V. Design and characterization of poly(glycerol-sebacate)-co-poly(caprolactone) (PGS-co-PCL) and its nanocomposites as novel biomaterials: The promising candidate for soft tissue engineering. *Eur. Polym. J.* **2020**, *138*, No. 109985.
(34) Perin, G. B.; Felisberti, M. I. Enzymatic Synthesis of Poly(glycerol sebacate): Kinetics, Chain Growth, and Branching Behavior. *Macromolecules* **2020**, *53* (18), 7925−7935.

https://doi.org/10.1021/acsabm.3c00894
ACS Appl. Bio Mater. 2024, 7, 863−878

(35) Chen, Y.; Miller, P. G.; Ding, X.; Stowell, C. E. T.; Kelly, K. M.; Wang, Y. Chelation Crosslinking of Biodegradable Elastomers. *Adv. Mater.* **2020**, *32*, No. 2003761.
(36) Xie, R.; Weisen, A. R.; Lee, Y.; Aplan, M. A.; Fenton, A. M.; Masucci, A. E.; Kempe, F.; Sommer, M.; Pester, C. W.; Colby, R. H.; Gomez, E. D. Glass transition temperature from the chemical structure of conjugated polymers. *Nat. Commun.* **2020**, *11* (1), 893.
(37) Kong, Y.; Hay, J. N. The enthalpy of fusion and degree of crystallinity of polymers as measured by DSC. *Eur. Polym. J.* **2003**, *39* (8), 1721−1727.
(38) Lanyi, F. J.; Wenzke, N.; Kaschta, J.; Schubert, D. W. On the Determination of the Enthalpy of Fusion of α-Crystalline Isotactic Polypropylene Using Differential Scanning Calorimetry, X-Ray Diffraction, and Fourier-Transform Infrared Spectroscopy: An Old Story Revisited. *Adv. Eng. Mater.* **2020**, *22* (9), 1−8.
(39) Bandzierz, K.; Reuvekamp, L.; Dryzek, J.; Dierkes, W.; Blume, A.; Bielinski, D. Influence of Network Structure on Glass Transition Temperature of Elastomers. *Materials* **2016**, *9* (7), 607.
(40) Zhao, Y.; Ma, Y.; Xiong, Y.; Qin, T.; Zhu, Y.; Deng, H.; Qin, J.; Shi, X.; Zhang, G. Chemically crosslinked crystalline thermoplastic polyolefin elastomer with good elasticity and improved thermo-mechanical properties. *Polymer* **2022**, *254*, No. 125075.
(41) Malpani, D.; Majumder, A.; Samanta, P.; Srivastava, R. K.; Nandan, B. Supramolecular Route for Enhancing Polymer Electrospinnability. *ACS Omega* **2018**, *3* (11), 15666−15678.
(42) Xu, L.; Qiao, Y.; Qiu, D. Coordinatively Stiffen and Toughen Hydrogels with Adaptable Crystal-Domain Cross-Linking. *Adv. Mater.* **2023**, *35* (12), No. e2209913.
(43) Oesterreicher, A.; Ayalur-Karunakaran, S.; Moser, A.; Mostegel, F. H.; Edler, M.; Kaschnitz, P.; Pinter, G.; Trimmel, G.; Schlögl, S.; Griesser, T. Exploring thiol-yne based monomers as low cytotoxic building blocks for radical photopolymerization. *J. Polym. Sci., Part A: Polym. Chem.* **2016**, *54* (21), 3484−3494.
(44) Risley, B. B.; Ding, X.; Chen, Y.; Miller, P. G.; Wang, Y. Citrate Crosslinked Poly(Glycerol Sebacate) with Tunable Elastomeric Properties. *Macromol. Biosci.* **2021**, *21* (2), No. e2000301.
(45) Wang, Z.; Mithieux, S. M.; Vindin, H.; Wang, Y.; Zhang, M.; Liu, L.; Zbinden, J.; Blum, K. M.; Yi, T.; Matsuzaki, Y.; Oveissi, F.; Akdemir, R.; Lockley, K. M.; Zhang, L.; Ma, K.; Guan, J.; Waterhouse, A.; Pham, N. T. H.; Hawkett, B. S.; Shinoka, T.; Breuer, C. K.; Weiss, A. S. Rapid Regeneration of a Neoartery with Elastic Lamellae. *Adv. Mater.* **2022**, *34* (47), No. e2205614.
(46) Dobrin, P. B. Mechanical Properties of Arteries. *Physiol. Rev.* **1978**, *58* (2), 397−460.
(47) Turner, B.; Ramesh, S.; Menegatti, S.; Daniele, M. Resorbable elastomers for implantable medical devices: highlights and applications. *Polym. Int.* **2022**, *71* (5), 552−561.
(48) Dong, X.; Yuan, X.; Wang, L.; Liu, J.; Midgley, A. C.; Wang, Z.; Wang, K.; Liu, J.; Zhu, M.; Kong, D. Construction of a bilayered vascular graft with smooth internal surface for improved hemocompatibility and endothelial cell monolayer formation. *Biomaterials* **2018**, *181*, 1−14.
(49) Wu, Y. L.; D'Amato, A. R.; Yan, A. M.; Wang, R. Q.; Ding, X.; Wang, Y. Three-Dimensional Printing of Poly(glycerol sebacate) Acrylate Scaffolds via Digital Light Processing. *ACS Appl. Bio Mater.* **2020**, *3* (11), 7575−7588.
(50) Ding, X.; Wu, Y. L.; Gao, J.; Wells, A.; Lee, K.; Wang, Y. Tyramine functionalization of poly(glycerol sebacate) increases the elasticity of the polymer. *J. Mater. Chem. B* **2017**, *5* (30), 6097−6109.
(51) Woodard, L. N.; Grunlan, M. A. Hydrolytic Degradation and Erosion of Polyester Biomaterials. *ACS Macro Lett.* **2018**, *7* (8), 976−982.
(52) Zhou, G.; Groth, T. Host Responses to Biomaterials and Anti-Inflammatory Design-a Brief Review. *Macromol. Biosci.* **2018**, *18* (8), No. e1800112.
(53) Chen, J. L.; Steele, T. W. J.; Stuckey, D. C. Metabolic reduction of resazurin; location within the cell for cytotoxicity assays. *Biotechnol. Bioeng.* **2018**, *115* (2), 351−358.
(54) Dokuchaeva, A. A.; Timchenko, T. P.; Karpova, E. V.; Vladimirov, S. V.; Soynov, I. A.; Zhuravleva, I. Y. Effects of Electrospinning Parameter Adjustment on the Mechanical Behavior of Poly-epsilon-caprolactone Vascular Scaffolds. *Polymers* **2022**, *14* (2), 349.
(55) Sun, H.; Mei, L.; Song, C.; Cui, X.; Wang, P. The in vivo degradation, absorption and excretion of PCL-based implant. *Biomaterials* **2006**, *27* (9), 1735−1740.
(56) Ulery, B. D.; Nair, L. S.; Laurencin, C. T. Biomedical Applications of Biodegradable Polymers. *J. Polym. Sci. B Polym. Phys.* **2011**, *49* (12), 832−864.
(57) Pappalardo, D.; Mathisen, T.; Finne-Wistrand, A. Biocompatibility of Resorbable Polymers: A Historical Perspective and Framework for the Future. *Biomacromolecules* **2019**, *20* (4), 1465−1477.
(58) Santoro, M.; Shah, S. R.; Walker, J. L.; Mikos, A. G. Poly(lactic acid) nanofibrous scaffolds for tissue engineering. *Adv. Drug Delivery Rev.* **2016**, *107*, 206−212.
(59) Miyachi, H.; Tara, S.; Otsuru, S.; Yi, T.; Lee, Y.-U.; Drews, J. D.; Nakayama, H.; Miyamoto, S.; Sugiura, T.; Shoji, T.; Breuer, C. K.; Shinoka, T. Imatinib attenuates neotissue formation during vascular remodeling in an arterial bioresorbable vascular graft. *JVS: Vascular Science* **2020**, *1*, 57−67.
(60) Tara, S.; Kurobe, H.; Rocco, K. A.; Maxfield, M. W.; Best, C. A.; Yi, T.; Naito, Y.; Breuer, C. K.; Shinoka, T. Well-organized neointima of large-pore poly(l-lactic acid) vascular graft coated with poly(l-lactic-co-ε-caprolactone) prevents calcific deposition compared to small-pore electrospun poly(l-lactic acid) graft in a mouse aortic implantation model. *Atherosclerosis* **2014**, *237* (2), 684−691.
(61) de Valence, S.; Tille, J. C.; Mugnai, D.; Mrowczynski, W.; Gurny, R.; Möller, M.; Walpoth, B. H. Long term performance of polycaprolactone vascular grafts in a rat abdominal aorta replacement model. *Biomaterials* **2012**, *33* (1), 38−47.
(62) Bergmeister, H.; Seyidova, N.; Schreiber, C.; Strobl, M.; Grasl, C.; Walter, I.; Messner, B.; Baudis, S.; Frohlich, S.; Marchetti-Deschmann, M.; Griesser, M.; di Franco, M.; Krssak, M.; Liska, R.; Schima, H. Biodegradable, thermoplastic polyurethane grafts for small diameter vascular replacements. *Acta biomaterialia* **2015**, *11*, 104−113.
(63) Wu, W.; Allen, R. A.; Wang, Y. Fast-degrading elastomer enables rapid remodeling of a cell-free synthetic graft into a neoartery. *Nat. Med.* **2012**, *18* (7), 1148−1153.
(64) Allen, R. A.; Wu, W.; Yao, M.; Dutta, D.; Duan, X.; Bachman, T. N.; Champion, H. C.; Stolz, D. B.; Robertson, A. M.; Kim, K.; Isenberg, J. S.; Wang, Y. Nerve regeneration and elastin formation within poly(glycerol sebacate)-based synthetic arterial grafts one-year post-implantation in a rat model. *Biomaterials* **2014**, *35* (1), 165−173.
(65) Lee, K. W.; Gade, P. S.; Dong, L.; Zhang, Z.; Aral, A. M.; Gao, J.; Ding, X.; Stowell, C. E. T.; Nisar, M. U.; Kim, K.; Reinhardt, D. P.; Solari, M. G.; Gorantla, V. S.; Robertson, A. M.; Wang, Y. A biodegradable synthetic graft for small arteries matches the performance of autologous vein in rat carotid arteries. *Biomaterials* **2018**, *181*, 67−80.

https://doi.org/10.1021/acsabm.3c00894
ACS Appl. Bio Mater. 2024, 7, 863−878